nature aging

Article

https://doi.org/10.1038/s43587-025-00869-3

Activation of AMPK by GLP-1R agonists mitigates Alzheimer-related phenotypes in transgenic mice

Received: 12 October 2024

Accepted: 7 April 2025

Published online: 20 May 2025

Check for updates

Yun Zhang[1,2,10] ✉, Huaqiu Chen[2,10], Yijia Feng[3,4,10], Mingjing Liu[5], Zhi Lu[6], Bolang Hu[3,4], Lifen Chen[4], Yang Zhang[7], Jiawen Liu[2], Fang Cai[4], Yifan Zhao[3,4], Wenhao Pan[3,4], Xinxin Liao[8], Sipei Pan[4], Isabel Bestard-Lorigados[9], Yili Wu[3,4] & Weihong Song[3,4,9] ✉

Individuals with type 2 diabetes mellitus have an increased risk of developing Alzheimer's disease (AD). GLP-1 receptor agonists (GLP-1RAs) are used for glycemic control in diabetes and show potential neuroprotective properties, but their effects on AD and the underlying mechanisms are not well understood. Here we demonstrate that GLP-1RAs can alleviate AD-related phenotypes by activating 5′ AMP-activated protein kinase (AMPK) signaling. We found that plasma GLP-1 levels were decreased in AD model mice and negatively correlated with amyloid-beta (Aβ) load in patients with AD. Enhancing GLP-1 signaling through GLP-1RAs increased CaMKK2–AMPK signaling, which subsequently reduced BACE1-mediated cleavage of amyloid precursor protein (APP) and Aβ generation. GLP-1RAs also increased AMPK activity in microglia, inhibiting neuroinflammation and promoting Aβ phagocytosis. Consequently, GLP-1RAs inhibited plaque formation and improved memory deficits in AD model mice. Our findings indicate that AMPK activation mediates the effects of GLP-1RAs on AD, highlighting the therapeutic potential of GLP-1RAs for the treatment of AD.

Alzheimer's disease (AD) is the most prevalent form of dementia, and neuritic plaques, neurofibrillary tangles and neuronal loss are the hallmarks of AD neuropathology[1]. Amyloid β (Aβ) protein, the principal component of plaques, is generated through cleavages of amyloid precursor protein (APP) by β-secretase and γ-secretase[2]. Beta-site APP cleaving enzyme 1 (BACE1) is the β-secretase cleaving APP at two β-sites, Asp+1 and Glu+11, within the Aβ domain to generate the membrane-bound APP C-terminal fragments (CTFs) C99 and C89, respectively[3,4]. Subsequently, γ-secretase cleaves C99, leading to the release of Aβ and the CTFγ[5,6].

Individuals with type 2 diabetes mellitus (T2DM) have an increased risk of developing AD[7,8]. Impaired glucose homeostasis in the brain plays an important role in AD pathogenesis[9–12]. Individuals may develop insulin resistance and impaired glucose metabolism more than 10 years before the occurrence of Alzheimer's symptoms, suggesting that insulin resistance and glucose metabolism could serve as a biomarker for early diagnosis of the disease[13,14]. Impaired insulin signaling and high glucose also disrupts both the processing of APP and the clearance of Aβ[15,16]. Reduced neuronal glucose uptake is associated with hyperphosphorylation of tau proteins, compromised synaptic plasticity, deficits in neurotransmitters and the initiation of inflammatory cascades, leading to neurodegenerative disease[17]. These findings have raised the possibility that anti-diabetic medication may provide therapeutic benefits for AD[18].

Glucagon-like peptide-1 (GLP-1) is an incretin hormone[19]. It is produced through cleavages of the proglucagon peptide by prohormone convertase 1/3 (PC1/3) and prohormone convertase 2 (PC2)[20]. After its generation, GLP-1 (1–37) undergoes further processing to release

A full list of affiliations appears at the end of the paper. ✉e-mail: zhangyun_202104@163.com; weihong@wmu.edu.cn

two active forms: GLP-1 (7–36) amide and GLP-1 (7–37)[21]. Secreted by intestinal L-cells in response to food intake, GLP-1 plays a key role in glucose metabolism and homeostasis[22]. GLP-1 receptor (GLP-1R) is a G-protein-coupled receptor (GPCR) predominantly expressed in pancreatic islet β-cells as well as in the brain, heart, gastrointestinal tract and kidney[23]. The receptor features a large N-terminal extracellular domain connected to seven α-helices by three extracellular and intracellular loops, along with a C-terminal intracellular helix[24]. Upon binding to GLP-1R, GLP-1 exerts its effects, including enhancing insulin secretion, reducing glucagon levels and increasing feelings of fullness[25]. These actions collectively contribute to lower blood glucose levels, making GLP-1 signaling a key target for modification of T2DM.

Glucagon-like peptide-1 receptor agonists (GLP-1RAs), such as liraglutide, semaglutide and exenatide, mimic the action of GLP-1 and have a prolonged half-life, positioning them as first-line or second-line medications for lowering blood glucose levels in patients with T2DM. Clinical studies demonstrated that GLP-1RAs effectively lower hemoglobin A1c levels and promote weight loss in individuals with T2DM[26,27]. Recent studies showed that GLP-1RA reduces the risk of neurodegenerative diseases, such as AD. Data from a large Danish registry-based cohort study involving 120,054 patients revealed a lower incidence of dementia among those treated with GLP-1RAs[28]. A phase 2 clinical trial in over 200 patients with mild cognitive impairments or AD showed that liraglutide decreased neuronal loss[29]. Several studies indicated that GLP-1RAs, including liraglutide, exenatide and lixisenatide, reduce Aβ accumulation, tau hyperphosphorylation and neuroinflammation[30–33]. However, the mechanisms underlying these effects remain elusive.

In the present study, we found a reduction of GLP-1 levels in AD and a correlation between plasma GLP-1 levels and brain energy metabolism as well as neuropathology in patients with AD. Administration of GLP-1RAs increases calcium/calmodulin-dependent protein kinase kinase (CaMKK) activity, which further activates 5′ AMP-activated protein kinase (AMPK) signaling to increase fatty acid oxidation (FAO), oxidative phosphorylation (OXPHOS), glycolysis and adenosine triphosphate (ATP) synthesis in brain cells. The GLP-1RA-induced AMPK activation decreases Aβ production by modulating *BACE1* expression via nuclear factor kappa B (NF-κB) signaling. GLP-1RAs promote Aβ phagocytosis by activation of AMPK in microglia. Consequently GLP-1RA treatment reduces neuritic plaque formation and improves cognitive deficits in AD transgenic mice, providing evidence that activating AMPK by GLP-1RAs could represent an effective therapeutic strategy for AD.

Results

Plasma GLP-1 is reduced and linked to Aβ load in AD

To explore the role of GLP-1 in the pathogenesis of AD, we conducted a comparative analysis of plasma GLP-1 levels between wild-type (WT) mice and the AD transgenic mice APP23/PS45 (refs. 34,35). We found that plasma GLP-1 levels in APP23/PS45 were significantly reduced to nearly half of those in WT mice ($P = 0.0288$; Fig. 1a), along with reduced glucose uptake (Fig. 1b) and ATP generation in neurons derived from AD mice (Fig. 1c). Furthermore, we observed a reduction in the expression (Fig. 1d,e and Extended Data Fig. 1a,b) and membrane translocation (Fig. 1d,f) of glucose transporter 3 (GLUT3), which is the primary glucose transporter in neurons. Considering that approximately 20% of the brain's total energy consumption is derived from FAO[36], we performed a Seahorse XF96 Cell Mito Stress Test to measure the oxygen consumption rate (OCR) and ATP production in astrocytes (Fig. 1g,h and Extended Data Figs. 2 and 3). Compared to WT mice, AD mice exhibited reductions in basal respiration, maximal respiration and spare respiratory capacity, ultimately resulting in a decrease in OXPHOS-dependent ATP synthesis (Fig. 1h). Using ^{18}F-AV45 positron emission tomography (PET) imaging to evaluate brain amyloid load in patients with AD, we identified a strong negative correlation between plasma GLP-1 levels and Aβ plaque accumulation in the hippocampus ($R = -0.825$, $P = 0.0017$; Fig. 1i). Among the participants, the individual with the lowest plasma GLP-1 level (4.22 pg ml^{-1}) exhibited a significantly higher hippocampal amyloid load (standardized uptake value ratio (SUVR) = 1.44) compared to the individual with the highest plasma GLP-1 level (19.23 pg ml^{-1}), who had an SUVR of 0.87 (Fig. 1j). These findings suggest that lower plasma GLP-1 levels are associated with increased amyloid burden in the hippocampus.

Next, we administered exendin-4, a GLP-1RA, to enhance GLP-1 signaling, which successfully restored glucose uptake capacity (Fig. 1b) and ATP generation (Fig. 1c) in AD neurons as well as FAO (Fig. 1g,h and Extended Data Figs. 2 and 3) in AD astrocytes. However, exendin-4 treatment did not have an impact on glycolysis in AD astrocytes (Extended Data Fig. 4). Exendin-4 also alleviated the AD-induced reductions in the levels of GLUT3 and the mitochondrial regulator peroxisome proliferator-activated receptor γ co-activator 1α (PGC-1α) (Fig. 1d–f and Extended Data Fig. 1c,d). We then further explored the impact of exendin-4 on neuronal glycolysis and OXPHOS by conducting OCR and extracellular acidification rate (ECAR) analysis. The results revealed that, after the improvement in glucose uptake, exendin-4 treatment notably enhanced both OXPHOS (Extended Data Fig. 5a–e) and glycolytic capacity (Extended Data Fig. 5f–i) in AD neurons. In addition, we assessed cellular metabolites such as pyruvate and reactive oxygen species (ROS). Exendin-4 did not alter pyruvate levels (Extended Data Fig. 5j) but significantly reduced the AD-induced increase in ROS, indicating its role in preventing excessive OXPHOS (Extended Data Fig. 5k,l). Furthermore, we observed that the administration of compound C, a widely used AMPK inhibitor, counteracted the beneficial effects of exendin-4, suggesting that the actions of exendin-4 are closely linked to AMPK activity (Fig. 1b–h and Extended Data Figs. 1–3 and 5).

GLP-1RA enhances CaMKK2-mediated AMPK phosphorylation

To examine the effect of GLP-1 signaling on AMPK activity, primary neurons isolated from WT mouse embryos (embryonic day (E) 17) were treated with exendin-4 or tirzepatide, a dual gastric inhibitory polypeptide (GIP)/GLP-1R co-agonist[37]. Treatment with exendin-4 at concentrations of 0.25 μM, 0.5 μM and 1 μM significantly increased the levels of phosphorylated AMPK to 251.2% ± 7.9% ($P = 0.0006$),

Fig. 1 | Plasma GLP-1 levels are associated with disturbed brain energy metabolism and Aβ pathology. a, Plasma samples were collected from WT and APP23/PS45 AD transgenic mice to measure GLP-1 levels. Twelve mice (six males and six females) of each group. A two-tailed Student's *t*-test was performed for statistical analysis. Primary neurons were isolated from embryonic WT and APP23 AD mice (E17) and subjected to glucose uptake assay (**b**) as well as ATP production assay (**c**). $n = 3$ independent experiments. One-way ANOVA followed by Tukey's multiple comparisons test was performed for statistical analysis. **d**, Immunocytochemistry was performed for measuring GLUT3 expression. Images were acquired using a Zeiss Apotome. The regions within the box were enlarged and displayed in the bottom line with intensity traces (indicated by white offset lines). Scale bar, 5 μm. The expression (**e**) and translocation (**f**) of GLUT3 in neurons were quantified. $n = 10$ cells from two independent experiments. One-way ANOVA followed by Tukey's multiple comparisons test was performed for statistical analysis. Primary astrocytes isolated from embryonic WT and APP23 AD mice (E17) were used for a Seahorse XF96 Cell Mito Stress Test to measure OCR (**g** and **h**). $n = 3$ independent experiments. One-way ANOVA followed by Tukey's multiple comparisons test was performed for statistical analysis. Twelve patients with AD (six males and six females) underwent ^{18}F-AV45 PET/MR scans to assess brain amyloid load, and their blood samples were collected to measure plasma GLP-1 levels. **i**, The correlation between plasma GLP-1 levels and brain Aβ pathology in patients with AD was analyzed. **j**, ^{18}F-AV45 PET/MR images of the patient with the lowest plasma GLP-1 level (Patient 1: 4.22 pg ml^{-1}) and the patient with the highest plasma GLP-1 level (Patient 2: 19.23 pg ml^{-1}) are presented. All the results are expressed as mean ± s.e.m. C.C, compound C; EX-4, exendin-4.

https://doi.org/10.1038/s43587-025-00869-3

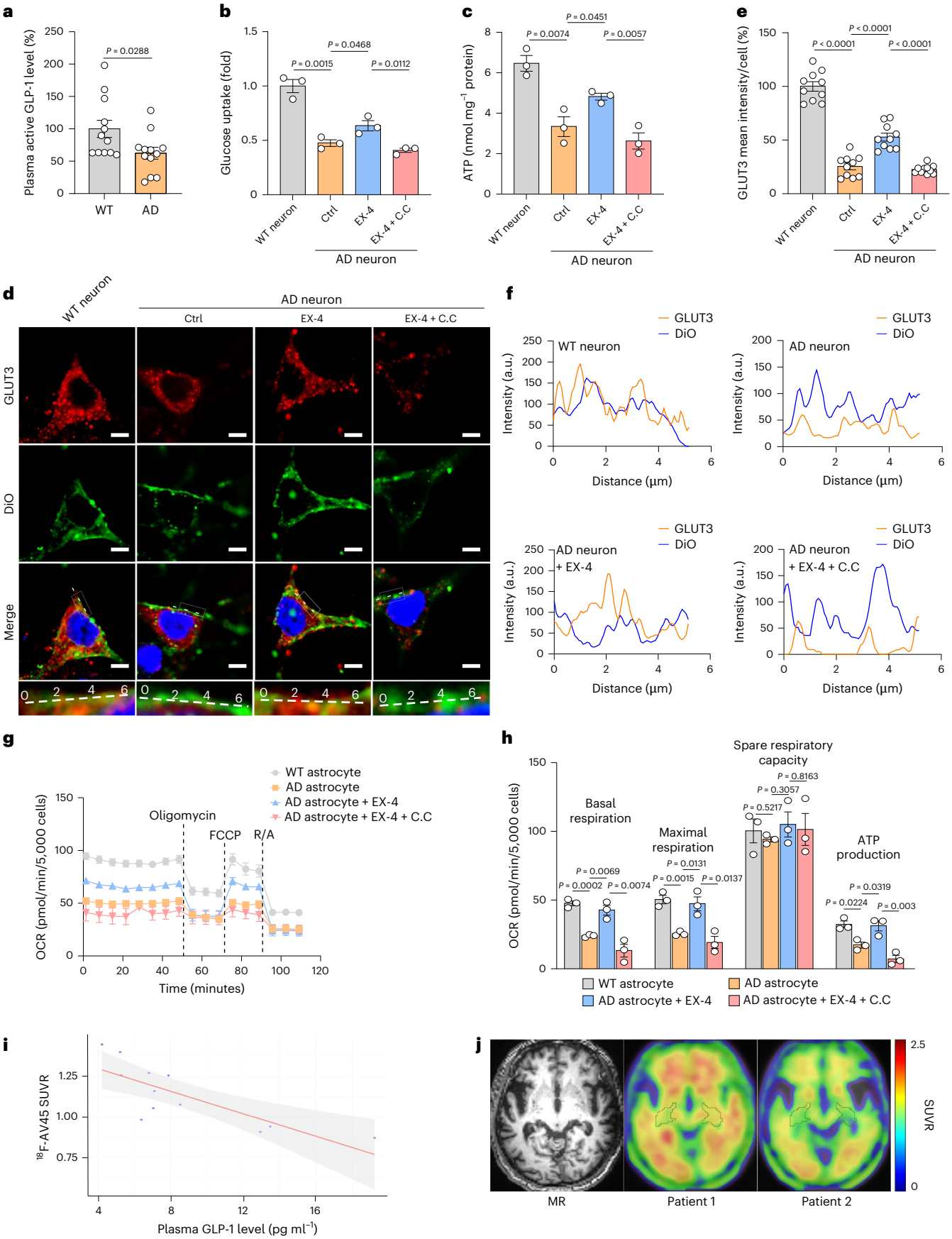

https://doi.org/10.1038/s43587-025-00869-3

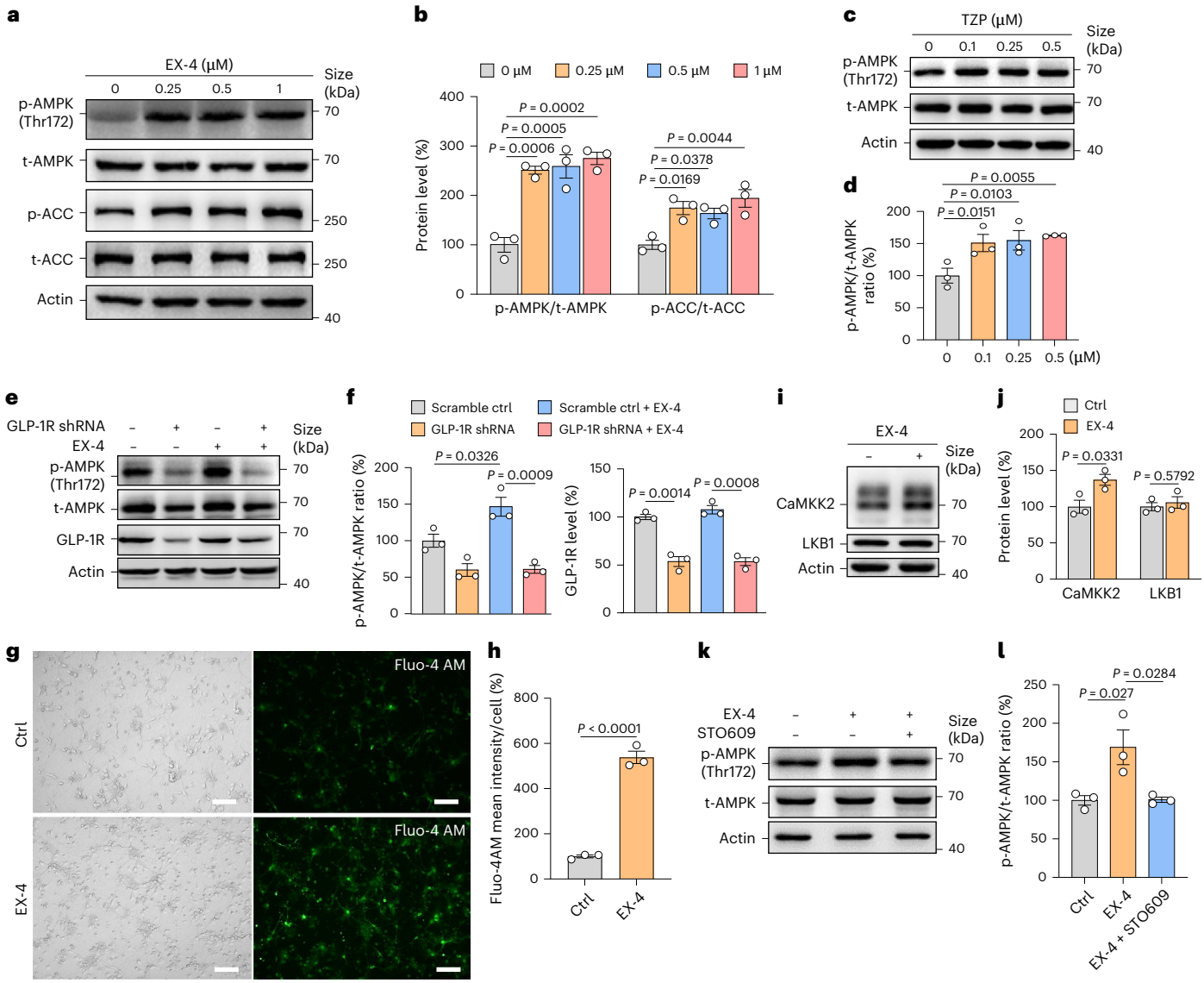

Fig. 2 | GLP-1RAs induce AMPK phosphorylation via Ca^{2+}-mediated CaMKK2 activation. Primary neurons isolated from WT mouse embryos were cultured and treated with different doses of exendin-4 (**a** and **b**) and tirzepatide (**c** and **d**) for 24 h. Cell lysates were subjected to western blot analysis for detecting phosphorylated AMPK, phosphorylated ACC, total AMPK and total ACC. β-actin was detected as the internal control. $n = 3$ independent experiments. One-way ANOVA followed by Dunnett's multiple comparisons test was performed for statistical analysis. **e**,**f**, Primary neurons were transduced with a lentiviral shRNA vector to reduce the expression of GLP-1Rs and then treated with or without exendin-4. Control shRNA lentivirus was used as a negative control. Phosphorylated AMPK, total AMPK and GLP-1R were detected by performing immunoblot analysis. $n = 3$ independent experiments. One-way ANOVA followed by Tukey's multiple comparisons test was performed for statistical analysis. **g**,**h**, Primary WT mouse neurons were labeled with Fluo-4 AM to measure intracellular Ca^{2+}. Green fluorescent signals were analyzed. Scale bar, 100 μm. $n = 3$ independent experiments. A two-tailed Student's t-test was performed for statistical analysis. **i**,**j**, Primary WT mouse neurons were treated with exendin-4 and subjected to immunoblot for detecting CaMKK2 and LKB1 levels. $n = 3$ independent experiments. A two-tailed Student's t-test was performed for statistical analysis. **k**,**l**, Primary WT mouse neurons were treated with exendin-4 with or without STO609, a CaMKK2 inhibitor. Cell lysates were subjected to western blot analysis for detecting phosphorylated AMPK and total AMPK. β-actin was detected by anti-actin antibody AC-15 as the internal control. $n = 3$ independent experiments. One-way ANOVA followed by Tukey's multiple comparisons test was performed for statistical analysis. All the results are expressed as mean ± s.e.m. EX-4, exendin-4; TZP, tirzepatide.

258.9% ± 23.7% ($P = 0.0005$) and 275.0% ± 12.5% ($P = 0.0002$), respectively (Fig. 2a,b). The activation of AMPK resulted in a further increase in the levels of phosphorylated acetyl-CoA carboxylase (ACC) to 174.5% ± 13.3% ($P = 0.0169$), 163.5% ± 10.8% ($P = 0.0378$) and 194.1% ± 17.9 ($P = 0.0044$), respectively (Fig. 2a,b). Similarly, tirzepatide at 0.1 μM, 0.25 μM and 0.5 μM also markedly elevated the levels of phosphorylated AMPK to 150.9% ± 13.4% ($P = 0.0151$), 155.1% ± 15.1% ($P = 0.0103$) and 162.2% ± 0.5% ($P = 0.0055$), respectively (Fig. 2c,d). To confirm that these effects of GLP-1RAs were dependent on the binding of GLP-1 to its receptors GLP-1R, primary neurons were transduced with a lentiviral short hairpin RNA (shRNA) vector to knock down GLP-1R expression. Inhibition of GLP-1R expression resulted in a diminished response to GLP-1RAs (Fig. 2e,f). It is known that elevated intracellular calcium levels trigger AMPK phosphorylation, a process mediated by CaMKK2 (ref. 38). Treatment with exendin-4 significantly enhanced calcium influx into the neurons (Fig. 2g,h), which further increased CaMKK2 levels to 137.1% ± 7.5% ($P = 0.0331$) (Fig. 2i,j). Furthermore, the application of STO609, a CaMKK inhibitor, significantly attenuated the effect of exendin-4 on AMPK phosphorylation (Fig. 2k,l). Liver kinase B1 (LKB1) is recognized to directly phosphorylate threonine 172 (Thr172)

https://doi.org/10.1038/s43587-025-00869-3

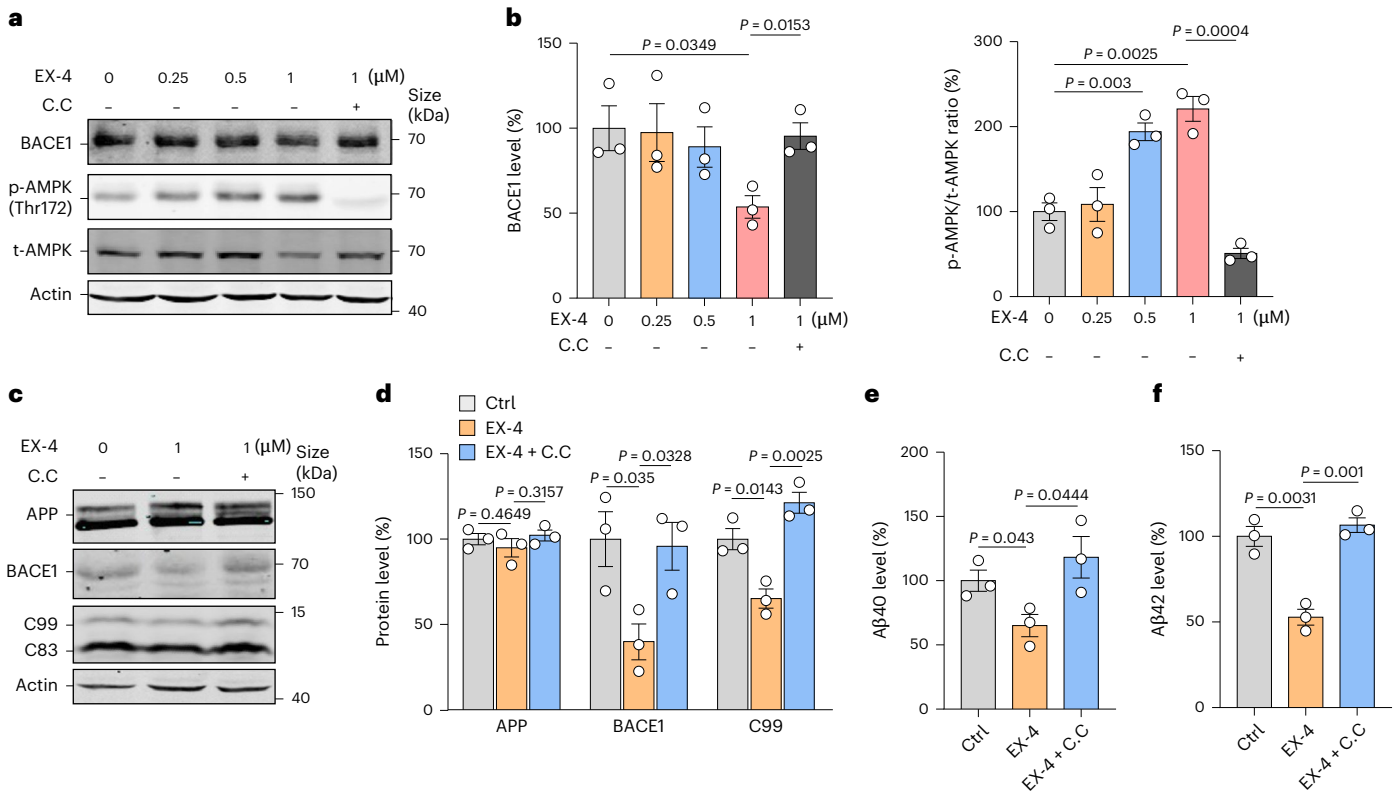

Fig. 3 | AMPK phosphorylation reduces BACE1-mediated APP processing. **a**,**b**, Primary WT mouse neurons were treated with different doses of exendin-4 with or without compound C, an AMPK inhibitor. Western blot analysis was performed for detecting endogenous BACE1, phosphorylated AMPK and total AMPK levels. β-actin was detected by anti-actin antibody AC-15 as the internal control. $n = 3$ independent experiments. One-way ANOVA followed by Tukey's multiple comparisons test was performed for statistical analysis. **c**,**d**, Swedish mutant APP stable cell line 20E2 was cultured and treated with exendin-4 with or without compound C to inhibit AMPK activity. Full-length APP and the APP CTFs were detected with C20 antibody. Endogenous BACE1 was detected with anti-BACE1 antibody. β-actin was detected by anti-actin antibody AC-15 as the internal control. $n = 3$ independent experiments. One-way ANOVA followed by Tukey's multiple comparisons test was performed for statistical analysis. Aβ ELISA was conducted to detect Aβ40 (**e**) and Aβ42 (**f**) in conditioned medium from 20E2 cells. $n = 3$ independent experiments. One-way ANOVA followed by Tukey's multiple comparisons test was performed for statistical analysis. All the results are expressed as mean ± s.e.m. C.C, compound C; EX-4, exendin-4.

of AMPKα[39]. Our findings indicated that GLP-1RAs had no significant effect on LKB1 expression ($P = 0.5729$) (Fig. 2i,j). These results suggest that GLP-1RAs enhance AMPK activity through a mechanism mediated by CaMKK2.

AMPK phosphorylation by GLP-1RA reduces BACE1 and Aβ production

It was reported that GLP-1RAs modulate Aβ metabolism[40]. However, the exact mechanisms, particularly the role of AMPK signaling, remain unclear. We found that exendin-4 at a concentration of 1 μM significantly reduced BACE1 levels in both primary mouse neurons and the human Swedish mutant APP stable cell line 20E2 to 53.6% ± 6.6% ($P = 0.0349$) (Fig. 3a,b) and 39.8% ± 10.5% ($P = 0.035$) (Fig. 3c,d), respectively. The treatment significantly decreased the levels of the β-secretase cleavage product APP C99 to 65.2% ± 5.6% ($P = 0.0143$) (Fig. 3c,d). However, exendin-4 treatment did not have a significant effect on APP expressions ($P = 0.4649$) (Fig. 3c,d). To assess the levels of Aβ40 and Aβ42 in the conditioned media of 20E2 cells, an Aβ ELISA was performed. Exendin-4 markedly reduced the levels of Aβ40 and Aβ42 to 65.1% ± 8.7% ($P = 0.043$) (Fig. 3e) and 52.8% ± 4.6% ($P = 0.0031$) (Fig. 3f), respectively. In contrast, the addition of compound C to inhibit AMPK activity significantly diminished the effects of exendin-4 on BACE1 expression (Fig. 3a–d) as well as C99 and Aβ production (Fig. 3c–f). To confirm our results, we further infected primary APP23 mouse neurons with AMPK-targeted shRNA and found that reduction of AMPK expression markedly mitigated the impact of exendin-4 on BACE1-mediated APP processing (Extended Data Fig. 6a,b) and Aβ generation (Extended Data Fig. 6c). In addition, by inhibiting FAO in AD astrocytes, we observed a notable alteration of the effect of exendin-4 on BACE1 expression (Extended Data Fig. 2f,g) as well as the amyloidogenic process of APP for Aβ generation (Extended Data Fig. 2h). Furthermore, we also demonstrated the effect of exendin-4 on AKT and PKA signaling, which, along with AMPK signaling, regulated BACE1 expression (Extended Data Fig. 2i–k). These findings clearly demonstrate that exendin-4 inhibited BACE1-mediated APP processing to generate Aβ and the effects, at least in part, mediated by AMPK activity.

NF-κB mediates AMPK-induced transcription of *BACE1*

To determine how AMPK regulates BACE1 expression, we first conducted a *BACE1* gene promoter assay for its transcriptional regulation. The *BACE1* promoter construct pB1-luc was constructed by cloning the human *BACE1* promoter region spanning from −1,942 bp to +292 bp into the promoterless vector pGL3-basic upstream of the firefly luciferase reporter gene[35,41] (Fig. 4a). N2a cells were transfected with the promoter construct and were subsequently treated with an AMPK inhibitor (compound C) or an AMPK activator (5-aminoimidazole-4-carboxamide ribonucleoside (AICAR)). Inhibition of AMPK signaling by compound C at 50 μM or 100 μM significantly elevated the promoter activity to 343.5% ± 28.0% ($P = 0.0011$) and 499.8% ± 33.7% ($P = 0.0003$), respectively (Fig. 4a). In contrast, boosting AMPK activity with AICAR treatment at 1 mM or 2 mM markedly reduced the promoter activity to 60.7% ± 2.1% ($P = 0.0061$) and 50.7% ± 1.8% ($P = 0.0026$), respectively

https://doi.org/10.1038/s43587-025-00869-3

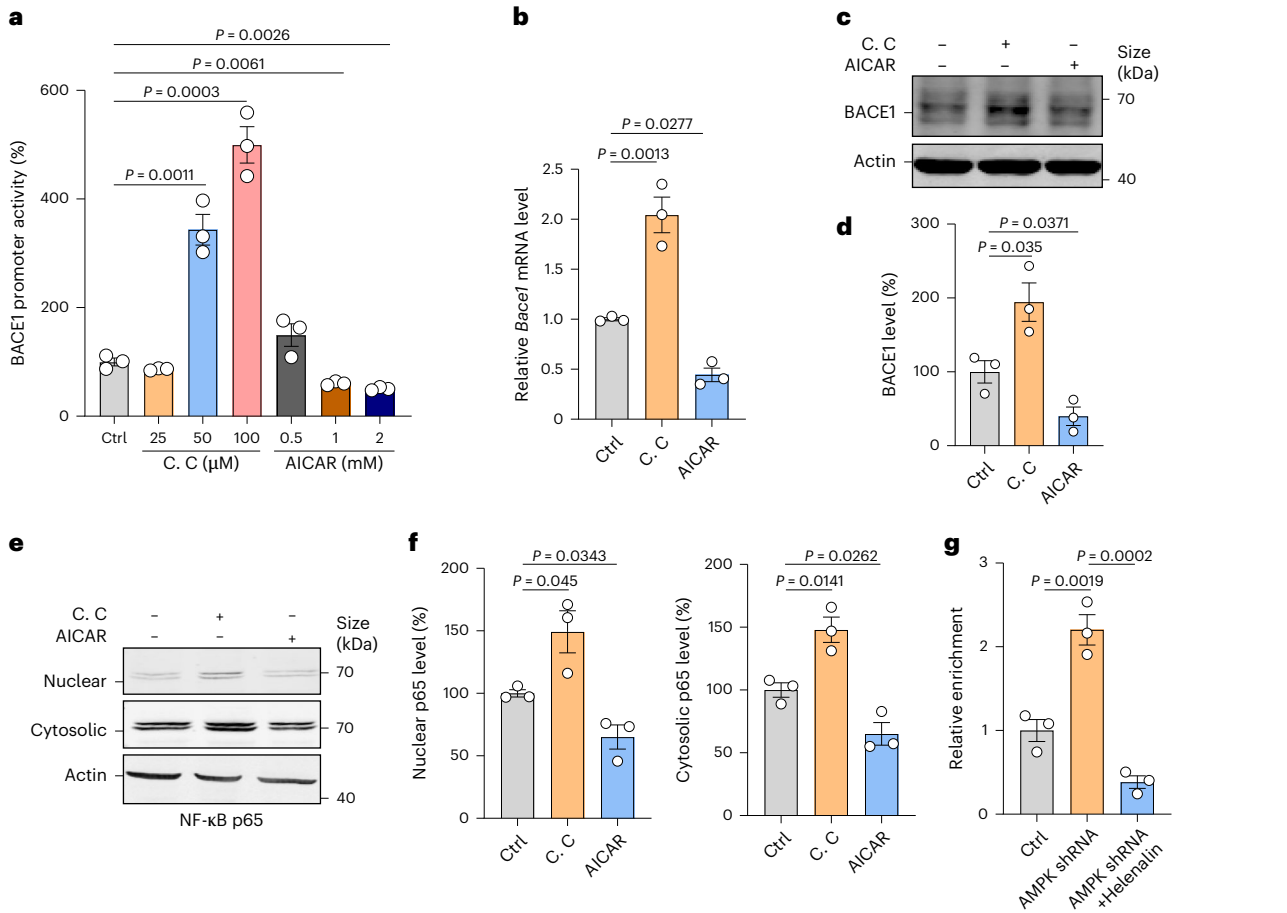

Fig. 4 | AMPK regulation of BACE1 transcription is dependent on NF-κB p65 activity. a, The human *Bace1* promoter was transfected into N2a cells and treated with different doses of compound C or AICAR. AMPK activity regulated the luciferase activity. $n = 3$ independent experiments. One-way ANOVA followed by Dunnett's multiple comparisons test was performed for statistical analysis. Primary mouse neurons were treated with compound C or AICAR. **b**, RNA was extracted, and qPCR was performed to measure endogenous mouse BACE1 mRNA levels. One-way ANOVA followed by Dunnett's multiple comparisons test was performed for statistical analysis. **c**,**d**, Western blot analysis was performed to measure the levels of endogenous BACE1 proteins. $n = 3$ independent experiments. One-way ANOVA followed by Dunnett's multiple comparisons test was performed for statistical analysis. **e**, Primary APP23 mouse neurons were treated with compound C or AICAR for 24 h, followed by cell fractionation. Cytosolic and nuclear fractions were subjected to SDS-PAGE. AMPK activity regulated NF-κB p65 levels in the nuclear and cytosolic fraction (**f**). $n = 3$ independent experiments. One-way ANOVA followed by Dunnett's multiple comparisons test was performed for statistical analysis. N2a cells were infected with lentivirus carrying scramble sequence or shRNA sequence targeting AMPK, with or without the administration of helenalin, an inhibitor of NF-κB. **g**, A ChIP assay was performed to detect the binding of NF-κB with *Bace1* promoter. $n = 3$ independent experiments. One-way ANOVA followed by Tukey's multiple comparisons test was performed for statistical analysis. All the results are expressed as mean ± s.e.m. C.C, compound C.

(Fig. 4a). Consistently, inhibition of AMPK by compound C also increased the mRNA levels (Fig. 4b) and protein levels of BACE1 in primary mouse neurons (Fig. 4c,d), whereas stimulation of AMPK activity by AICAR significantly decreased the mRNA levels (Fig. 4b) and protein levels of BACE1 (Fig. 4c,d). Our previous study showed that NF-κB significantly enhanced the *BACE1* promoter activity[35,42]. To investigate whether the effect of AMPK on BACE1 expression is mediated by NF-κB, primary APP23 mouse neurons were treated with compound C or AICAR and then subjected to subcellular fractionation (Fig. 4e). Treatment with AICAR notably decreased nuclear NF-κB p65 levels to 65.0% ± 9.7% ($P = 0.0343$) compared to the control (Fig. 4f). Additionally, AICAR treatment also reduced cytosolic NF-κB p65 levels to 65.1% ± 8.9% ($P = 0.0262$) compared to the control (Fig. 4f). These findings indicate that activation of AMPK by AICAR leads to a reduction in NF-κB activity by lowering NF-κB p65 levels. Furthermore, we performed a chromatin immunoprecipitation (ChIP) assay, which demonstrated that the suppression of AMPK significantly enhanced the binding of NF-κB p65 to the *BACE1* promoter, leading to an increase in BACE1 expression (Fig. 4g). Overall, our results suggest that NF-κB signaling plays a role in mediating the regulatory effect of GLP-1RAs on *BACE1* gene expression.

GLP-1RAs–induced AMPK activation promotes microglial phagocytosis

We observed that GLP-1RAs, including exendin-4 and tirzepatide, also enhanced AMPK phosphorylation to 124.6% ± 6.1% ($P = 0.0132$) and 129.8% ± 4.0% ($P = 0.0056$) in the microglial cell line BV2, respectively (Fig. 5a,b). To identify the biological functions influenced by GLP-1RAs in microglia, RNA sequencing (RNA-seq) analyses were performed to detect differentially expressed genes (DEGs) between cells cultured with Aβ oligomers and those pre-treated with exendin-4 before being cultured with Aβ oligomers. Our results showed that exendin-4 treatment increased the expressions of genes associated with phagocytosis while reducing the expressions of disease-associated microglia (DAM) genes and genes related to inflammation (Fig. 5c). In addition, Gene Ontology (GO) and Kyoto Encyclopedia of Genes and Genomes (KEGG) pathway analyses were performed to further explore the biological process involved. Treatment with exendin-4 enhanced the expressions of

genes related to AMPK signaling pathway (Fig. 5d) and glucose metabolism, including genes involved in glucose catabolism, gluconeogenesis and glucose transmembrane transport (Fig. 5e). Furthermore, inflammation-related biological processes were also downregulated after exendin-4 treatment (Fig. 5f). To further validate the results of the RNA-seq analyses, we conducted immunocytochemistry (Fig. 5g–i) and western blot analyses (Extended Data Fig. 7). Exendin-4 or tirzepatide significantly increased expressions of cluster of differentiation 68 (CD68) (Fig. 5g,h and Extended Data Fig. 7a,b) and lysosomal-associated membrane protein 1 (LAMP1) (Fig. 5g,i and Extended Data Fig. 7a,c) in BV2 cells, two well-established markers for microglial phagocytosis and lysosomal degradation[43].

To further assess whether GLP-1RAs promote microglial phagocytosis, we measured the uptake of carboxyfluorescein (FAM)-labeled Aβ42 (FAM-Aβ42) by BV2 cells. Both exendin-4 and tirzepatide significantly enhanced the phagocytic activity of BV2 cells (Fig. 5j,k). Previous studies demonstrated that GLP-1RAs possess anti-inflammatory properties that may be beneficial for treating lung injury[44]. Our study found that GLP-1RAs also significantly reduced Aβ-induced inflammatory cytokines produced by BV2 cells, including decreases in interleukin (IL)-1β, IL-6 and tumor necrosis factor (TNF) (Extended Data Fig. 8a–c), while increasing the production of the anti-inflammatory cytokine TGF-β (Extended Data Fig. 8d). Moreover, the application of compound C to inhibit AMPK activity attenuated the effects of GLP-1RAs on neuroinflammation (Extended Data Fig. 8). These results suggest that the anti-inflammatory effects of GLP-1RAs are mediated through AMPK signaling.

GLP-1RAs regulate *BACE1* expression and Aβ production in vivo

To investigate the effect of GLP-1RAs on AMPK activity and APP processing in vivo, we first assessed AMPK phosphorylation, APP CTFs and Aβ production in the brain of APP23/PS45 mice. APP23/PS45 mice express both the familial AD-associated human Swedish mutant APP751 transgene and G384A mutant presenilin-1 (PS1) transgene, and the double transgenic mice developed neuritic plaques in the neocortex and hippocampus and cognitive impairments[34]. The mice were administered with exendin-4 (25 nmol kg^{-1}) daily for 8 weeks starting at 6 weeks of age, whereas age-matched control mice received a vehicle solution. Treatment with exendin-4 significantly increased the levels of phospho-AMPK proteins in the brain to 174.9% ± 20.6% ($P = 0.0186$) (Fig. 6a,b), which correlated with decreased levels of the β-secretase-generated C99 in both cortex (56.4% ± 3.5%, $P = 0.001$) and hippocampus (42.7% ± 3.4%, $P = 0.0006$) compared to controls (Fig. 6c,d). Compared to controls, the cortical levels of Aβ40 and Aβ42 in exendin-4-treated mice were reduced to 77.7% ± 5.7% ($P = 0.0055$) and 81.5% ± 4.3% ($P = 0.0034$), respectively (Fig. 6e). The hippocampal levels of Aβ40 and Aβ42 in exendin-4-treated mice were also decreased to 75.1% ± 4.9% ($P = 0.0009$) and 78.1% ± 4.4% ($P = 0.0021$), respectively (Fig. 6e). These results indicate that enhanced AMPK activity due to GLP-1RA treatment reduces β-secretase cleavage of APP and Aβ production in vivo.

Furthermore, we investigated whether the expression of BACE1 was affected by GLP-1RA treatment in vivo. Western blot analysis revealed that exendin-4 treatment significantly reduced the protein level of BACE1 in both cortex (58.7% ± 2.0%, $P = 0.0003$) and hippocampus (62.3% ± 7.1%, $P = 0.0102$), compared to control mice, with no significant impact on APP protein levels ($P > 0.05$) (Fig. 6c,d). Our in vitro study demonstrated that GLP-1RAs regulated the transcription of the *BACE1* gene. To confirm that the reduction in BACE1 protein levels in the brains of the exendin-4-treated mice was due to decreased *BACE1* gene transcription, the endogenous *Bace1* mRNA levels were measured (Fig. 6f). Exendin-4 treatment markedly reduced *Bace1* mRNA level to 0.36 ± 0.14 ($P = 0.0052$), whereas no significant change was observed in the *App* mRNA level (Fig. 6f). Furthermore, AD mice were injected with exendin-4 in conjunction with compound C to inhibit AMPK activity. The results demonstrated that the inhibition of AMPK activity notably alleviated the impact of exendin-4 on the regulation of BACE1 expression and BACE1-mediated amyloidogenic processing of APP in both the cortex and hippocampus (Extended Data Fig. 9). These findings indicate that, in line with the in vitro findings, GLP-1RAs inhibit *BACE1* gene expression and its β-secretase activity in vivo through the regulation of AMPK activity.

GLP-1RAs reduce AD pathology and cognitive deficits in mice

To investigate the specific effect of GLP-1RAs on AD pathogenesis, 4G8 immunostaining and thioflavin S staining were used to detect Aβ-containing neuritic plaques in the brain of APP23/PS45 mice (Fig. 7a). Treatment with exendin-4 significantly decreased plaque numbers to approximately half in APP23/PS45 mice compared to the vehicle-treated group (18.9 ± 1.4 versus 35.2 ± 2.0 per slice, $P < 0.0001$; Fig. 7b). We further found that exendin-4 treatment markedly reduced the levels of pro-inflammatory cytokines in mouse brains, with IL-1β, IL-6 and TNF levels decreasing to 83.3% ± 1.8% ($P = 0.0008$), 70.0% ± 2.5% ($P < 0.0001$) and 48.1% ± 2.4 ($P < 0.0001$), respectively (Extended Data Fig. 10a–d). In addition, there was an increase in CD68 expression with the treatment of exendin-4 (Extended Data Fig. 10e,f). To assess the impact of exendin-4 treatment on cognitive deficits, we conducted a Morris water maze test after 8 weeks of exendin-4 treatment in APP23/PS45 mice. In the visible platform trials, both exendin-4-treated and control APP23/PS45 mice exhibited similar escape latencies (29.2 ± 1.5 s versus 28.8 ± 1.8 s, $P = 0.8691$) (Fig. 7c) and path lengths (4.5 ± 0.2 m versus 3.9 ± 0.4 m, $P = 0.2525$) (Fig. 7d), indicating that exendin-4 treatment did not affect mouse mobility or visual acuity. During the hidden platform trials, mice treated with exendin-4 showed significant improvements compared to the vehicle-treated controls. The escape latencies on the fourth and fifth days of the hidden platform trials were shorter (30.2 ± 2.9 s and 29.9 ± 2.8 s) for the exendin-4-treated mice than that of the vehicle-treated mice (40.0 ± 2.8 s and 42.3 ± 2.8 s) (Fig. 7e). In addition, the exendin-4-treated mice swam shorter distances to reach the platform compared to the control mice on the fourth day (2.8 ± 0.3 m versus 5.3 ± 0.6 m, $P = 0.0007$) (Fig. 7f). In the probe trial on the final testing day, when the platform was removed, exendin-4 treatment notably improved the spatial memory in the APP23/PS45

Fig. 5 | GLP-1RAs promote microglial phagocytosis and inhibit neuroinflammation. BV2 cells were treated with exendin-4 or tirzepatide for 24 h. **a**,**b**, Western blot analysis was performed for detecting phosphorylated AMPK and total AMPK levels. β-actin was detected by anti-actin antibody AC-15 as the internal control. $n = 3$ independent experiments. One-way ANOVA followed by Dunnett's multiple comparisons test was performed for statistical analysis. BV2 cells cultured with Aβ oligomers or pre-treated with exendin-4 before being cultured with Aβ oligomers. After RNA extraction, the samples were used for the RNA-seq analyses. **c**, DEGs were measured by using DESeq2 (version 1.40.2) with the default parameters. **d**–**f**, GO and KEGG pathway analyses were performed to explore the biological process. Total samples = 6. One-sided hypergeometric test was used, and the Benjamini–Hochberg method was employed to control the false discovery rate for multiple comparisons. BV2 cells were treated with exendin-4 or tirzepatide for 24 h. **g**–**i**, Immunocytochemistry was performed. Images were acquired using a Zeiss microscope. Scale bar, 20 μm. $n = 6$ images from three independent experiments for quantifications. One-way ANOVA followed by Dunnett's multiple comparisons test was performed for statistical analysis. **j**,**k**, The uptake of FAM-labeled Aβ42 (FAM-Aβ42) by BV2 cells was measured. Scale bar, 20 μm. $n = 8$ images from three independent experiments for quantifications. One-way ANOVA followed by Dunnett's multiple comparisons test was performed for statistical analysis. All the results are expressed as mean ± s.e.m. BP, biological process; EX-4, exendin-4; TZP, tirzepatide.

https://doi.org/10.1038/s43587-025-00869-3

https://doi.org/10.1038/s43587-025-00869-3

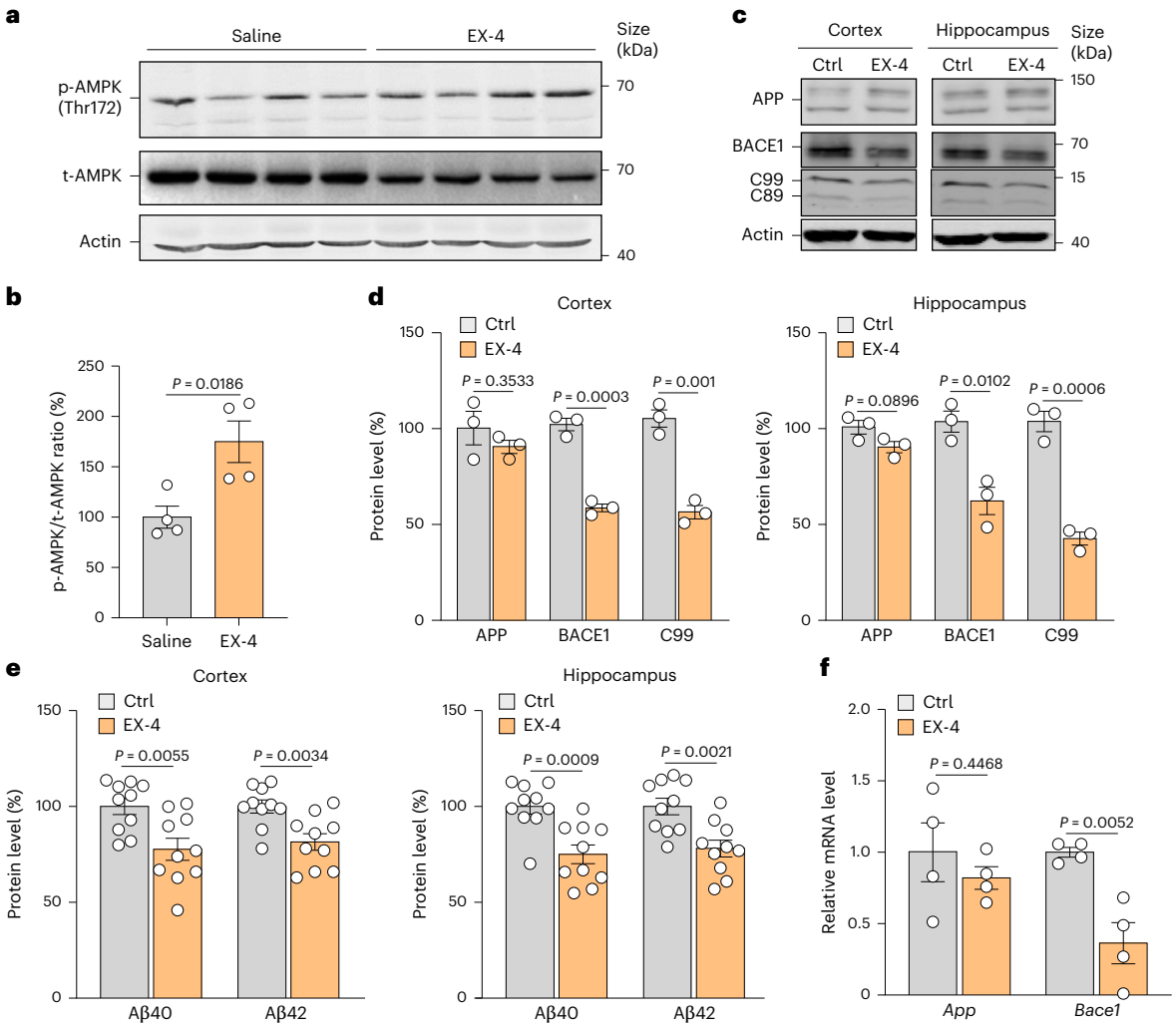

Fig. 6 | GLP-1RAs inhibit BACE1 cleavage of APP and Aβ production in vivo. Hemi-brains from exendin-4-treated and control APP23/PS45 mice ($n = 36$ mice total) were homogenized in RIPA-Doc lysis buffer and separated with 8% Tris-glycine or 16% Tris-tricine SDS-PAGE. Phosphorylated AMPK and total AMPK levels (**a** and **b**) as well as full-length APP, APP CTFs (C99 and C89) and endogenous BACE1 levels were detected (**c** and **d**). β-actin was detected by anti-actin antibody AC-15 as the internal control. A two-tailed Student's *t*-test was performed for statistical analysis. **e**, ELISA was performed to measure Aβ40 and Aβ42 levels from the brain tissues of APP23/PS45 mice injected with or without exendin-4. $n = 10$ for each group. A two-tailed Student's *t*-test was performed for statistical analysis. Total RNA was isolated from APP23/PS45 mouse cortices. **f**, Sets of gene-specific primers were used to amplify *App* and *Bace1* genes. qPCR was performed. β-actin was used as an internal control. $n = 4$ for each group. A two-tailed Student's *t*-test was performed for statistical analysis. All the results are expressed as mean ± s.e.m. EX-4, exendin-4.

mice, as evidenced by the increased number of entries into the third quadrant, where the hidden platform was previously located (3.7 ± 0.7 times versus 1.6 ± 0.4 times, $P = 0.0143$) (Fig. 7g). These results demonstrate that GLP-1RA treatment significantly ameliorated the cognitive impairments of the AD model mice.

Discussion

GLP-1RAs are known to regulate peripheral glucose and lipid metabolism[45,46]. However, their effect on energy metabolism within the brain and AD remains elusive. In the present study, we observed a significant negative correlation between peripheral GLP-1 levels and brain amyloid load in patients with AD. Lower levels of GLP-1 during AD were associated with impaired glucose uptake, decreased FAO and reduced ATP synthesis in brain cells. Notably, the administration of GLP-1RAs (exendin-4 and tirzepatide) to enhance GLP-1 signaling effectively restored the disturbed energy metabolism in AD brains, consistent with a report that liraglutide and thapsigargin restored OXPHOS and glycolysis in dopaminergic-like neurons under chronic ER stress[47]. Mechanistically we found that GLP-1RAs promoted CaMKK2-induced activation of AMPK, a key cellular energy sensor, resulting in decreased Aβ production by neurons and an increase in Aβ phagocytosis by microglia. Consequently, treatment with GLP-1RAs significantly inhibited neuritic plaque formation and improved cognitive deficits in the AD model mice (Fig. 7h).

GLP-1RAs are synthetic analogs of GLP-1, a gut-derived peptide hormone that plays a vital role in lowering blood glucose levels[48]. This effect is achieved through the stimulation of insulin secretion in response to an oral glucose intake, a process known as the incretin effect[49]. Unlike natural GLP-1 peptides, these synthetic analogs are designed to resist degradation by the enzyme dipeptidyl peptidase 4 (DPP-4) for a prolonged half-life[50]. Exendin-4, a 39-amino-acid agonist of the GLP-1R derived from the saliva of the Gila monster (*Heloderma suspectum*)[51], has been clinically approved for the treatment of insulinoma and T2DM[52]. Tirzepatide, a dual GIP/GLP-1RA, was recently approved by the US Food & Drug Administration for T2DM management[37]. Beyond their glucose-lowering effects, GLP-1RAs also modulate the release of various neurotransmitters, including serotonin, dopamine, GABA and glutamate, which may influence

https://doi.org/10.1038/s43587-025-00869-3

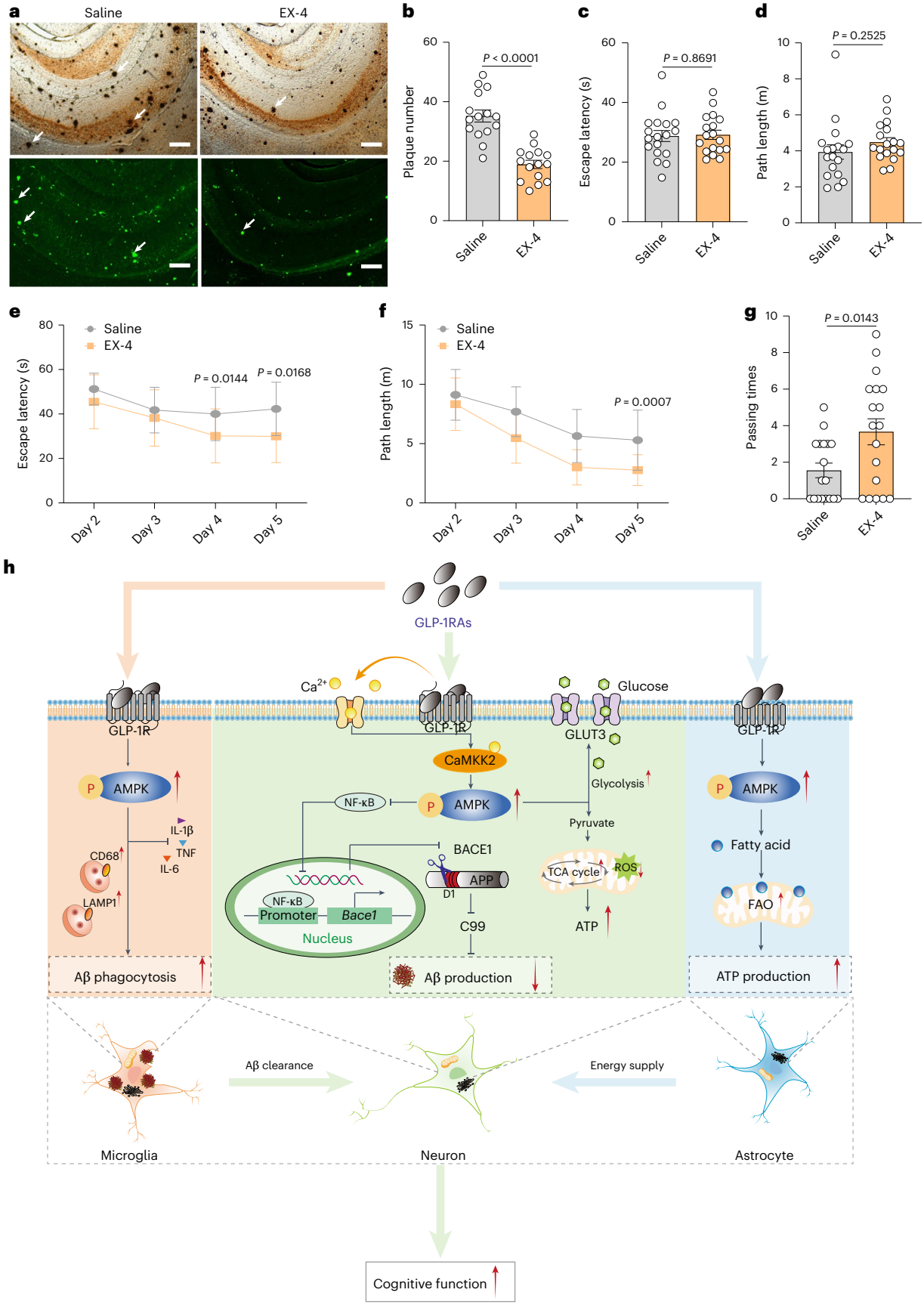

Fig. 7 | Exendin-4 treatment significantly reduces neuritic plaque formation and improves memory deficits in AD transgenic mice. Neuritic plaques were detected using 4G8 antibody and thioflavin S fluorescent staining. **a**, Representative brain sections of the control and exendin-4-injected APP23/PS45 mice. White arrows point to plaques. Scale bar,100 μm. **b**, Quantification of neuritic plaques; the number represents mean ± s.e.m., $n = 30$ mice total, two-tailed Student's *t*-test. A Morris water maze test was conducted ($n = 36$: 18 exendin-4 treated and 18 sham treated). During the first day of visible platform tests, the exendin-4-treated and control APP23/PS45 mice exhibited a similar latency (**c**) and swimming distances (**d**) to escape onto the visible platform. $P > 0.05$, Student's *t*-test. In hidden platform tests, mice were trained with five trials per day for 4 d. APP23/PS45 mice treated with exendin-4 showed a shorter latency to escape onto the hidden platform on the third and fourth days (**e**) and a shorter swimming length before escaping onto the hidden platform on the fourth days (**f**). Tukey's post hoc analysis was performed for statistical analysis. **g**, In the probe trial on the sixth day, the APP23/PS45 mice treated with exendin-4 traveled into the third quadrant, where the hidden platform was previously placed, significantly more times than controls. Student's *t*-test was performed for statistical analysis. **h**, Summary graph. All the results are expressed as mean ± s.e.m.

cognitive function[53–56]. Our research revealed that both exendin-4 and tirzepatide significantly reduced Aβ plaque formation and improved cognitive deficit in AD model mice. These results are consistent with previous studies indicating that liraglutide, another GLP-1 RA, enhances the population of hippocampal CA1 neurons, decreases Aβ levels and inhibits tau tangle formation, leading to cognitive improvement in animal models[31,57,58].

As anti-diabetic medications, GLP-1RAs achieve glycemic control through various metabolic and energy-regulating mechanisms[59], and a recent study showed that GLP-1RA has a protective effect on kidney tubular by enhancing AMPK signaling, further activating FAO and inhibiting lipid synthesis and glycolysis[60]. The effects of AMPK on metabolism can be categorized into two main functions: inhibiting anabolic processes to reduce ATP consumption and stimulating catabolic processes to enhance ATP production[61]. During energy stress, activated AMPK promotes glucose uptake and lipid oxidation to generate energy while simultaneously shutting down energy-consuming processes, such as glucose and lipid synthesis, thereby restoring energy balance and maintaining homeostasis[62]. It was reported that AMPK inhibits tau phosphorylation and aggregation by either inhibiting GSK3β or facilitating tau deacetylation through the activation of SIRT1 (ref. 63). In addition, activation of AMPK by metformin improves mitochondrial function and cognitive deficits in AD models[64]. However, the impact of GLP-1RAs on AMPK activity and energy metabolism in brain cells remains largely unknown.

Reduced energy metabolism is an early feature of AD[65,66]. In our study, we found that exendin-4 and tirzepatide enhance CaMKK2-induced AMPK activation in brain cells. Deficiencies in glucose transporters, such as GLUT1 or GLUT3, can lead to impaired glucose uptake and metabolism in the brain, which may contribute to neurodegeneration[67]. Previous studies indicated the potential impact of GLP-1RAs on the expression of GLUT3 (refs. 68–70). In our study, we further found that activation of AMPK by GLP-1RAs elevated GLUT3 levels and facilitated its translocation to the membranes of neurons. This process resulted in enhanced glucose uptake by neurons, leading to increased glycolysis and OXPHOS for ATP synthesis. Furthermore, the increase in AMPK activity induced by GLP-1RA was associated with elevated expression of PGC-1α, a key regulator that stimulates mitochondrial biogenesis and enhances mitochondrial functions[71]. Mitochondrial dysfunction was implicated in AD pathogenesis[72]. Our findings indicated that GLP-1RA-induced AMPK activation also promoted FAO, leading to increased ATP production in astrocytes from AD model mice. AMPK plays a key role in the regulation of ketone bodies (KBs) derived from fatty acids in the astrocytes[73]. These KBs are transported to neurons via a monocarboxylate transporter and may serve as a direct antioxidant, thereby reducing mitochondrial ROS production[74,75]. Consistent with these findings, we found that exendin-4 significantly alleviated the AD-induced increase in ROS via phosphorylating AMPK, suggesting its potential in curbing excessive OXPHOS. The implication of this enhanced energy metabolism in astrocytes, as well as its potential impact on the astrocyte–neuron energy shuttle and its protective effects against fatty acid toxicity in neurons, warrants further investigations.

AMPK activity is reduced in the brains of patients suffering from AD[76]. This reduction facilitates the plaque and tangle formation, alterations in metabolic signaling and inflammation in the development of AD[77]. Leptin has been shown to decrease β-secretase activity and lower Aβ levels in vitro as well as to reduce Aβ accumulation in AD animal models, with these effects being at least partially mediated by AMPK[78]. Previous studies found that GLP-1RAs and GLP-1/GIP receptor agonists have an impact on the expression and activity of BACE1 (refs. 79,80). We found that GLP-1RAs reduced *BACE1* expression at the transcription level through AMPK activation. Our previous study demonstrated that NF-κB transcriptionally upregulates *BACE1* gene expression[35,42]. In the present study, we found that GLP-1RA-induced AMPK activation significantly reduced NF-κB p65 levels in the nuclear fraction of primary neurons. This phenomenon was also observed in the brains of mice with Parkinson's disease[81]. The cAMP/PKA/CREB and AKT signaling pathways are critical downstream effectors of GLP-1 signaling, regulating cellular metabolism and cell survival[82]. Our findings demonstrate that these two signaling pathways interact and cross-talk with AMPK to coordinately regulate BACE1 expression, providing insights into the molecular mechanisms underlying GLP-1-mediated effects. In addition, AMPK was identified as a crucial factor in facilitating the polarization of microglia from a pro-inflammatory to an anti-inflammatory phenotype[83]. We observed that GLP-1RA-induced AMPK activation in microglia inhibited the inflammation and, importantly, promoted phagocytosis. Furthermore, GLP-1RAs increased the expressions of CD68 and LAMP1, the markers associated with phagocytosis and lysosomal degradation[43]. Enhancement of microglial phagocytosis to reduce Aβ level could be a valid avenue for treatment of AD[84].

GLP-1RAs have emerged as a promising therapeutic strategy for AD[85]. In this study, we demonstrate their beneficial effects on AD. More importantly, we demonstrate GLP-1RAs as activators of AMPK in regulating energy metabolism and the function of brain cells to inhibit BACE1-mediated amyloidogenesis and cognitive impairments. This regulation serves as a key mechanism underlying their therapeutic effects on AD. Our findings provide valuable insights into the potential of GLP-1RAs as a therapeutic approach for AD and offer a timely mechanistic foundation to support further clinical trials.

Methods

Study approval

For human studies, written informed consent was obtained from all participants without any compensation. The study was approved by the Ethics Committee of the First Affiliated Hospital of Dalian Medical University (PJ-KS-KY-2023-149). Animals were cared for in accordance with the Guidelines and Principles of Laboratory Animal Care and the standard procedures established by the Ethics Committee of Wenzhou Medical University (wydw2022-0563). All animal experimental protocols were conducted in accordance with the regulations of the Institutional Animal Care and Use Committee of Wenzhou Medical University.

Sex as a biological variable

Our study examined male and female patients and animals, and similar findings are reported for both sexes.

Patients with AD and ^{18}F-AV45 PET

AD was diagnosed by at least two specialists, following the criteria of the National Institute of Neurological and Communicative Disorders and Stroke (NINCDS)–Alzheimer's Disease and Related Disorders Association (ADRDA). All participants underwent a comprehensive collection of medical history and clinical examination of the nervous system. Patients were excluded based on the following criteria: (1) clinical conditions such as diabetes mellitus, epilepsy, stroke or long-term use of medications known to cause progressive cognitive dysfunction; (2) Hachinski Ischemic Score (HIS) > 4 points, Hamilton Anxiety Rating Scale (HAMA) score ≥ 7 points and Hamilton Depression Rating Scale (HAMD) score ≥ 7 points; and (3) presence of severe heart, liver, lung, kidney or other organ diseases. A total of 12 patients with AD (six males and six females) underwent an ^{18}F-AV45 PET/MR scan (United Imaging). The ^{18}F-AV45 imaging agent was synthesized by the AllinOne module (Trasis), with the ^{18}F labeling of its corresponding precursor by the Department of Nuclear Medicine of the First Affiliated Hospital of Dalian Medical University. Changes in Aβ load in each brain area were quantitatively analyzed by using NeuroQ software (version 3.7).

ELISA quantification of human plasma GLP-1 concentrations

Twenty micoliters of dipeptidyl peptidase IV (DDP IV) inhibitor (Millipore Sigma, cat. no. DPP4-010) was added into the EDTA tubes to inhibit the degradation of GLP-1. Blood samples were obtained from each patient under fasting conditions and subsequently subjected to centrifugation at 1,000*g* for 10 min. The plasma was aliquoted, immediately frozen and kept at −80 °C. Plasma concentration of GLP-1 was determined by a human GLP-1 ELISA kit (Thermo Fisher Scientific, cat. no. EH221RB).

Cell culture, transfection and treatment

Cells were cultured at 37 °C in an incubator with 5% CO_2. HEK293 (human embryonic kidney), N2a (mouse neuroblast) and BV2 (mouse microglial) cells were maintained in high-glucose DMEM (Cytiva, cat. no. SH30243.01) supplemented with 10% FBS (Gibco, cat. no. 12483020) and 100 U ml^{-1} penicillin–streptomycin (Gibco, cat. no. 15140122). Transfection was carried out using polyethylenimine (MedChemExpress, cat. no. HY-K2014) for HEK cells and Lipofectamine 2000 reagent (Invitrogen, cat. no. 11668019) for N2a cells as previously described[86]. The 20E2 cell line is a Swedish mutant APP695 stable HEK293 cell line cultured in complete DMEM with 50 μg ml^{-1} geneticin. For the treatment, HEK cells and N2a cells were transfected in a 6-cm master plate and then split into 4 × 35-mm plates 4 h after transfection, maintained overnight (16 h) before treatment. Primary neurons were derived from WT and APP23 mice at E17 and cultured in neurobasal medium (Gibco, cat. no. 21103049) supplemented with B27 (Gibco, cat. no. 17504044) and GlutaMAX (Gibco, cat. no. 35050061). Primary astrocytes were also derived from WT and APP23 mice at E17 and were maintained in high-glucose DMEM. The culture medium was enriched with 10% FBS (Gibco, cat. no. 10270106). Primary neurons were infected with lentivirus carrying scramble sequence or shRNA sequence targeting GLP-1R or AMPK. Cells were treated with Aβ42 peptide (Millipore Sigma, cat. no. PP69), exendin-4 (Millipore Sigma, cat. no. 141758-74-9), tirzepatide (Selleck Chemicals, cat. no. LY3298176), compound C (Sigma-Aldrich, cat. no. 171260), AICAR (Sigma-Aldrich, cat. no. A9978), helenalin (MedChemExpress, cat. no. HY-119970) or STO609 (MedChemExpress, cat. no. HY-19805).

Preparation of Aβ oligomers

The lyophilized Aβ42 peptide was first monomerized by dissolving it to a final concentration of 1 mM in 100% hexafluoroisopropanol (HFIP). The HFIP was subsequently evaporated under vacuum using a SpeedVac, and the resulting peptide film was stored at −20 °C. For oligomeric Aβ, the peptide film was resuspended in dimethyl sulfoxide (DMSO), followed by ultrasonic treatment in a water bath for 10 min. The solution was then diluted to a final concentration of 100 μM in cold phenol-free F-12 cell culture media and incubated at 4 °C for 24 h.

Luciferase assay

BACE1 promoter construct pB1-luc (−1,942 to +292) was transfected into N2a cells, along with the *Renilla* (sea pansy) luciferase vector pCMV-Rluc for normalization of transfection efficiency. A luciferase assay was conducted 48 h after transfection using the Dual-Luciferase Reporter Assay System (Promega).

ChIP

A ChIP assay was conducted using a Pierce agarose ChIP kit (Thermo Fisher Scientific, cat. no. 26156). N2a cells were cross-linked in 1% formaldehyde (Sigma-Aldrich, cat. no. 252549), and DNA was fragmented to 200–600 bp in length through enzyme digestion. Each 500 μl of sheared chromatin was immunoprecipitated using 5 μl of monoclonal anti-NF-κB p65 (Cell Signaling Technology, cat. no. 8242S) or IgG control overnight at 4 °C. Input and immunoprecipitated samples were digested with proteinase K to reverse the cross-linking at 65 °C for 90 min. DNA was purified and further analyzed through quantitative polymerase chain reaction (qPCR) by using the primers against the *BACE1* promoter.

qPCR analysis

RNA was isolated using a FastPure Cell/Tissue Total RNA Isolation Kit v2 (Vazyme, cat. no. RC112-01). A HiScript III 1st Strand cDNA Synthesis Kit (Vazyme, cat. no. R312-01) was used to synthesize the first-strand cDNA following the manufacturer's instructions. cDNA was added to a reaction mix (20 μl final volume) containing gene-specific primers and Taq Pro Universal SYBR qPCR Master Mix (Vazyme, cat. no. Q712). All samples were run in duplicates and were analyzed with LightCycler 480 System. The relative gene expression was normalized to *Actin* controls. Primer sequences and information are as follows: BACE1 forward 5′-GGAACCCATCTCGGCATCC and reverse 5′-TCCGATTCCTCGTCGGTCTC; APP forward 5′-TCCG AGAGGTGTGCTCTGAA and reverse 5′-CCACATCCGCCGTAAAAGAATG; ACTIN forward 5′-CATTGCTGACAGGATGCAGAAGG and reverse 5′-TGCTGGAAGGTGGACAGTGAGG.

Immunoblot analysis

Brain tissues or cells were homogenized in RIPA lysis buffer (1% Triton X-100, 1% sodium deoxycholate, 4% SDS, 0.15 M NaCl, 0.05 M Tris-HCl, pH 7.2), supplemented with sodium orthovanadate (200 mM), β-glycerophosphate (25 mM), sodium pyrophosphate (20 mM), sodium fluoride (30 mM), phenylmethylsulfonyl fluoride (PMSF, 1 mM) and a complete Mini Protease Inhibitor Cocktail Tablet (Roche Diagnostics, cat. no. 04693159001)[35]. The samples were diluted in 4× SDS sample buffer, boiled and resolved on 10% or 12% Tris-glycine SDS-PAGE or 16% Tristricine SDS-PAGE, followed by transfer to nitrocellulose membranes. For immunoblot analysis, membranes were blocked for 1 h in PBS containing 5% nonfat dried milk, followed by overnight incubation at 4 °C in primary antibodies with shaking. Rabbit anti-APP C-terminal polyclonal antibody C20 was used to detect APP and its CTF products. BACE1 was detected with the anti-BACE1 antibody 208 recognizing the C-terminal end (Abcam, cat. no. ab183612; 1:1,000). Total AMPK was determined using a rabbit anti-AMPKα antibody (Cell Signaling Technology, cat. no. 2532S; 1:1,000). Phosphorylated AMPK was determined using a rabbit anti-phospho-AMPKα (Thr172) antibody (Cell Signaling Technology, cat. no. 2535S; 1:1,000). The NF-κB p65 subunit was determined using mouse anti-p65 (Sigma-Aldrich, cat. no. 8242S; 1:1,000). GLP-1Rs were determined using mouse monoclonal anti-GLP-1R antibody (Santa Cruz Biotechnology, cat. no. sc-390774; 1:500). CaMKK2 and LKB1 expressions were determined using rabbit anti-CaMKK2 antibody (Cell Signaling Technology, cat. no. 16810S; 1:1,000) and rabbit anti-LKB1 antibody (Thermo Fisher Scientific, cat.

no. PA5-96062; 1:500), respectively. CD68 was determined by rabbit anti-CD68 antibody (Proteintech, cat. no. 28058-1-AP; 1:1,000). LAMP1 was determined by rabbit anti-LAMP1 antibody (Cell Signaling Technology, cat. no. 99437S; 1:1,000). GLUT3 and PGC-1α were determined by rabbit polyclonal anti-GLUT3 antibody (Proteintech, cat. no. 20403-1-AP; 1:1,000) and mouse monoclonal anti-PGC-1α antibody (Proteintech, cat. no. 66369-1-Ig; 1:1,000). Internal control β-actin was analyzed using monoclonal antibody AC-15 (Sigma-Aldrich, cat. no. A5441; 1:8,000). The next day, membranes were incubated with IRDye 680-labeled or IRDye 800CW-labeled secondary antibodies (LI-COR Biosciences) for 1 h at room temperature. The membranes were then visualized using the LI-COR imaging system.

ELISA measurement for Aβ, mouse GLP-1 and inflammatory cytokines

HEK293 cells stably expressing the human APP gene with the Swedish mutation were cultured in medium supplemented with 1% FBS. After 24 h of exendin-4 treatment, with or without the AMPK inhibitor compound C, conditioned medium was collected, and protease inhibitors along with AEBSF (Roche Diagnostics, cat. no. 101500) were added to prevent Aβ peptide degradation. Cortical tissues from APP23/PS45 double transgenic mouse were prepared following the manufacturer's protocol before performing the ELISA protocol. The concentrations of Aβ40 and Aβ42 were measured using an Aβ1–40 or Aβ1–42 Colorimetric ELISA kit (Invitrogen, cat. nos. KHB3544 and KHB3481), in accordance with the manufacturer's guidelines. The plasma concentration of GLP-1 in 12-week-old APP23/PS45 and WT mice was measured using a mouse GLP-1 ELISA kit (Elabscience, cat. no. E-EL-M3012). BV-2 microglial conditioned medium was collected and centrifuged to remove particulates. APP23/PS45 double transgenic mouse cortical tissues were prepared according to the manufacturer's instructions. Levels of TNF (Elabscience, cat. no. E-EL-M3063), IL-6 (Elabscience, cat. no. E-EL-M0044), IL-1β (Elabscience, cat. no. E-EL-M0037) and TGF-β (Multi Sciences, cat. no. 70-EK981-96) in the culture medium or mouse cortical tissues were quantified using commercial ELISA kits.

Assessment of mitochondrial OXPHOS

The OCR was evaluated using a Seahorse XF96 flux analyzer (Agilent Technologies) in conjunction with the Seahorse XF Cell Mito Stress Test kit (Agilent Technologies, cat. no. 103015-100). Primary astrocytes and neurons isolated from APP23 mice were seeded with sequential injections of oligomycin (2 μM), FCCP (2 μM) and rotenone/antimycin A (R/A) (1 μM) to measure the OCR. To evaluate FAO, cells were incubated with Seahorse assay medium supplemented with palmitate (167 μM) and etomoxir (40 μM, HY-50202), an irreversible inhibitor of FAO.

Assessment of ECAR

The ECAR was measured like OCR in a Seahorse XF96 extracellular flux analyzer (Agilent Technologies), except that the neuronal medium was replaced with the XF DMEM (pH 7.4) medium without glucose, glutamine and pyruvate. After 1-h incubation in a CO_2-free incubator at 37 °C, ECAR was measured by sequentially injecting glucose, oligomycin and 2-deoxyglucose (2-DG). Basal glycolysis and glycolytic capacity were calculated and normalized to the concentration of protein in each corresponding microplate well measured by BCA protein assay (Thermo Fisher Scientific, cat. no. A55864).

Glucose uptake assay

To assess 2-DG uptake, the Glucose Uptake-Glo Assay (Promega, cat. no. J1341) was performed. Primary neurons were cultured on coverslips pre-coated with 10% poly-D-lysine (Solarbio, cat. no. P2100). After treatment, the cells were washed twice with PBS and then incubated with 1 mM 2-DG at room temperature for 10 min, followed by the sequential addition of stop buffer, neutralization buffer and detection buffer. Luminescence was measured using a plate reader (GloMax system).

ATP production assay

Neuronal ATP levels were measured using an ATP Assay Kit (Abcam, cat. no. ab83355). After the cells were washed with PBS twice, 100 μl of lysis buffer was added to each tube, which was then kept on ice. The lysate was centrifuged at 13,000*g* for 5 min at 4 °C. The supernatant was transferred to a new 1.5-ml tube for the ATP assay using the detection kit. The relative ATP level was calculated according to the following formula: relative ATP level = ATP value / protein value (nmol mg^{-1}).

ROS measurements

Changes in ROS levels were measured using a Cellular ROS Assay Kit (Abcam, cat. no. ab186027). In brief, primary neurons were plated onto 24-well confocal dishes that had been pre-coated with poly-D-lysine. After treatment with 1 μM exendin-4 for 24 h, the cells were washed once using PBS. Subsequently, 200 μl of ROS Red Stain working solution was added to each well, and the dishes were incubated for 30 min at 37 °C, protected from light. After incubation, the staining results were observed under a fluorescence microscope (excitation/emission (Ex/Em) = 520/605 nm).

Intracellular pyruvate quantification

Pyruvate was measured with a Pyruvate Assay Kit (Abcam, cat. no. ab65342). In brief, primary neurons were collected in assay buffer and exposed to a master mix with pyruvate oxidase, producing a fluorescent signal (Ex/Em = 535/587 nm) that directly reflected pyruvate levels. To inhibit the conversion of pyruvate to lactate, the samples were deproteinized using a 10-kDa cutoff spin filter (Pierce, cat. no. 88513). The pyruvate levels were then determined using a standard curve.

Phagocytosis assays

BV2 cells were treated with 1 μM exendin-4 or 0.5 μM tirzepatide for 24 h and then exposed to 10 μM cytochalasin D (MedChemExpress, cat. no. HY-N6682) or left untreated for 30 min, followed by 1-h incubation with 500 nM FAM-Aβ1–42 (AS-23525-05) oligomers. After treatment, cells were washed and fixed using 4% paraformaldehyde (PFA). The phagocytosis of FAM-labeled oAβ1–42 in BV2 cells was quantified through Leica confocal microscopy. The phagocytosis capacity was quantified by calculating the ratio of the cumulative fluorescent signal areas to the total count of phagocytic cells.

Live Fluo-4 AM calcium imaging

The measurement of intracellular calcium ion levels in neurons was facilitated by the Fluo-4 Calcium Assay Kit (Beyotime, cat. no. S1061S). Primary neurons were plated onto 24-well confocal dishes that had been pre-coated with poly-D-lysine. After treatment with 1 μM exendin-4 for 24 h, the cells were washed once using PBS. Subsequently, 250 μl of 1× Fluo-4 staining solution was added to each well, and the dishes were incubated for 30 min at 37 °C, protected from light. After incubation, the staining results were observed under a fluorescence microscope (Fluo-4 AM exhibits green fluorescence, Ex/Em = 490/525 nm).

RNA-seq and data processing

RNA-seq was performed on six independent RNA samples of BV2 cells: BV2 cells cultured with Aβ oligomers (three samples) and BV2 cells pre-treated with exendin-4 before being cultured with Aβ oligomers (three samples). After RNA extraction, the samples were passed quality control with Qubit 2.0 and a 2100 Bioanalyzer. Libraries were prepared using a TIANGEN Biotech kit and sequenced using an Illumina NovaSeq X Plus with PE150 mode. To measure DEGs, DESeq2 (version 1.40.2) with the default parameters was used. Gene set enrichment analysis (GSEA) of biological processes related to inflammation and glucose metabolism was conducted using the R package clusterProfiler (version 4.8.3), based on the results analyzed with the DESeq2 package and the GO database for Biological Process analysis. Absolute normalized enrichment score (NES) values greater than 1 and *P* values less than 0.05

were considered statistically significant. Based on the KEGG database, functional enrichment analysis was conducted using the R package clusterProfiler (version 4.8.3), with adjusted *P* values less than 0.05 considered statistically significant.

Transgenic mice and drug treatment

APP23 mice, which overexpress the Swedish APP751 (KM → NL) mutant transgene under the control of the mouse Thy1.2 promoter, were originally developed at Novartis Pharma as previously described[87]. APP23/PS45 double transgenic mice were generated by crossing APP23 mice with mice that overexpress the human G384A-mutated PS1 under the regulation of the murine Thy1 promoter (B6,D2-TgN(Thy1-PS1G384A)45)[35]. APP23 and PS45 mice were backcrossed to C57BL/6 mice for more than seven generations before breeding for the double transgenic mice. The genotype of the mice was confirmed by PCR using DNA from tail tissues. Although this mouse model does not fully capture the complexity of human AD, it provides valuable insights into amyloid-related mechanisms[35]. The treatment group contained 18 animals (nine females and nine males), and the sham-injected group contained 18 animals (nine females and nine males). No statistical methods were used to pre-determine sample sizes, but our sample sizes are similar to those reported in previous publications[35,88]. The treatment group received 25 nmol kg^{-1} exendin-4 with or without 20 mg kg^{-1} compound C diluted in 0.9% saline daily via intraperitoneal injection at the same time each day. Mice in the control group were injected with the vehicle solution containing DMSO diluted in 0.9% saline only. We tabulated the daily food consumption and weight for each mouse.

Immunohistochemical staining

Mice were euthanized after behavioral testing, and one hemisphere of the brains was quickly homogenized for protein, RNA or DNA extraction. The other hemisphere was fixed in 4% PFA and sectioned at 30-µm thickness using a Leica Cryostat. Every twelfth slice, maintaining the same reference position, was mounted onto slides for subsequent staining. Immunocytochemical staining was performed on floating sections. The plaques in the sections were detected with biotinylated monoclonal 4G8 antibody (BioLegend, cat. no. 800708) in 1:500 dilution, visualized by the ABC and DAB method and counted under a ×40 objective as previously described[88,89]. Plaques were quantified, and the average plaque count per slice was recorded for each mouse. Thioflavin S staining of plaques was performed with 1% thioflavin S visualized using fluorescence microscopy (Olympus). The brain slices were also stained by anti-CD68 (1:200; Proteintech, cat. no. 28058-1-AP). BV2 cells were fixed with 4% PFA and stained by anti-CD68 (1:200) or anti-LAMP1 (1:200; Cell Signaling Technology, cat. no. 99437S), followed by secondary antibodies. Primary neurons isolated from WT and APP23 mice were labeled with a cell plasma membrane staining kit with DiO (Byotime, cat. no. C1038) for 15 min and then fixed with 4% PFA and stained by anti-GLUT3 (1:400; Proteintech, cat. no. 20403010AP), followed by secondary antibodies. The staining results were viewed under the ×63 oil lens of the Zeiss fluorescence microscope.

Morris water maze test

The Morris water maze test was conducted as previously described[35]. APP23/PS45 mice treated with exendin-4 or saline (control group) underwent the Morris water maze test 1 d after the final injection. The test was carried out in a pool with a 10-cm-diameter platform positioned in the southeastern (SE) quadrant. During the visible platform test on the first day, the mice completed five consecutive trials, with a 60-min inter-trial interval. For the hidden platform trials, mice underwent five trials per day, with a 60-min rest between each trial. Each mouse was given up to 60 s to locate the platform. If the platform was not found within this time, the mouse was guided to the platform and allowed to rest for 15 s. On the final day, the probe trial was performed, in which the platform was removed and each mouse had 60 s to locate the platform's original position. Mouse behavior, including distance traveled, escape latency and the number of platform crossings, was recorded using automated video tracking (ANY-maze; Stoelting).

Statistics and reproducibility

All statistical analyses were performed using GraphPad Prism 7 software. All data were expressed as mean ± s.e.m. For two-group comparisons, statistical analysis was performed using a two-tailed Student's *t*-test. For multiple-group comparisons, results were analyzed by one-way ANOVA or two-way ANOVA followed by post hoc analysis where appropriate. Normality and equal variances were formally assessed to ensure that the assumptions of the test were met. Data collection and analysis were not performed blinded to the conditions of the experiments. Statistical significance was accepted when *P* values were less than 0.05.

Reporting summary

Further information on research design is available in the Nature Portfolio Reporting Summary linked to this article.

Data availability

The RNA-seq raw data are deposited in the Sequence Read Archive (https://www.ncbi.nlm.nih.gov/sra) with BioProject IDs PRJNA1227686, SRR32510895, SRR32510896, SRR32510897, SRR32510898, SRR32510899 and SRR32510900. All other data are available from the corresponding author upon reasonable request.

Code availability

The specific packages and versions used for analyzing RNA sequencing and data processing, including DESeq2 (version 1.40.2) and clusterProfiler (version 4.8.3), are explicitly stated in Methods. These packages are open source and are accessible through Bioconductor (https://www.bioconductor.org/packages/release/bioc/html/clusterProfiler.html; https://www.bioconductor.org/packages/release/bioc/html/DESeq2.html).

References

1. Zhang, Y., Chen, H., Li, R., Sterling, K. & Song, W. Amyloid β-based therapy for Alzheimer's disease: challenges, successes and future. *Signal Transduct. Target. Ther.* **8**, 248 (2023).
2. Zhang, Y. & Song, W. Islet amyloid polypeptide: another key molecule in Alzheimer's pathogenesis? *Prog. Neurobiol.* **153**, 100–120 (2017).
3. Deng, Y. et al. Amyloid-β protein (Aβ) Glu11 is the major β-secretase site of β-site amyloid-β precursor protein-cleaving enzyme 1(BACE1), and shifting the cleavage site to Aβ Asp1 contributes to Alzheimer pathogenesis. *Eur. J. Neurosci.* **37**, 1962–1969 (2013).
4. Zhang, S. et al. BACE1 cleavage site selection critical for amyloidogenesis and Alzheimer's pathogenesis. *J. Neurosci.* **37**, 6915–6925 (2017).
5. De Strooper, B. et al. Deficiency of presenilin-1 inhibits the normal cleavage of amyloid precursor protein. *Nature* **391**, 387–390 (1998).
6. Zhang, Z. et al. Presenilins are required for γ-secretase cleavage of β-APP and transmembrane cleavage of Notch-1. *Nat. Cell Biol.* **2**, 463–465 (2000).
7. Gudala, K., Bansal, D., Schifano, F. & Bhansali, A. Diabetes mellitus and risk of dementia: a meta-analysis of prospective observational studies. *J. Diabetes Investig.* **4**, 640–650 (2013).
8. Kang, Y. et al. Identification of circulating risk biomarkers for cognitive decline in a large community-based population in Chongqing China. *Alzheimers Dement.* **21**, e14443 (2025).
9. Rorbach-Dolata, A. & Piwowar, A. Neurometabolic evidence supporting the hypothesis of increased incidence of type 3 diabetes mellitus in the 21st century. *Biomed Res. Int.* **2019**, 1435276 (2019).

10. Nguyen, T. T., Ta, Q. T. H., Nguyen, T. K. O., Nguyen, T. T. D. & Giau, V. V. Type 3 diabetes and its role implications in Alzheimer's disease. *Int. J. Mol. Sci.* **21**, 3165 (2020).
11. Bano, D., Ehninger, D. & Bagetta, G. Decoding metabolic signatures in Alzheimer's disease: a mitochondrial perspective. *Cell Death Discov.* **9**, 432 (2023).
12. Yang, Y. & Song, W. Molecular links between Alzheimer's disease and diabetes mellitus. *Neuroscience* **250**, 140–150 (2013).
13. Mosconi, L. Brain glucose metabolism in the early and specific diagnosis of Alzheimer's disease. FDG-PET studies in MCI and AD. *Eur. J. Nucl. Med. Mol. Imaging* **32**, 486–510 (2005).
14. Arnold, S. E. et al. Brain insulin resistance in type 2 diabetes and Alzheimer disease: concepts and conundrums. *Nat. Rev. Neurol.* **14**, 168–181 (2018).
15. Delikkaya, B., Moriel, N., Tong, M., Gallucci, G. & de la Monte, S. M. Altered expression of insulin-degrading enzyme and regulator of calcineurin in the rat intracerebral streptozotocin model and human apolipoprotein E-ε4-associated Alzheimer's disease. *Alzheimers Dement. (Amst.)* **11**, 392–404 (2019).
16. Yang, Y., Wu, Y., Zhang, S. & Song, W. High glucose promotes Aβ production by inhibiting APP degradation. *PLoS ONE* **8**, e69824 (2013).
17. Lauretti, E., Li, J. G., Di Meco, A. & Pratico, D. Glucose deficit triggers tau pathology and synaptic dysfunction in a tauopathy mouse model. *Transl. Psychiatry* **7**, e1020 (2017).
18. Markowicz-Piasecka, M. et al. Metformin—a future therapy for neurodegenerative diseases. *Pharm. Res.* **34**, 2614–2627 (2017).
19. Kreymann, B., Williams, G., Ghatei, M. A. & Bloom, S. R. Glucagon-like peptide-1 7-36: a physiological incretin in man. *Lancet* **2**, 1300–1304 (1987).
20. Tucker, J. D., Dhanvantari, S. & Brubaker, P. L. Proglucagon processing in islet and intestinal cell lines. *Regul. Pept.* **62**, 29–35 (1996).
21. Sandoval, D. A. & D'Alessio, D. A. Physiology of proglucagon peptides: role of glucagon and GLP-1 in health and disease. *Physiol. Rev.* **95**, 513–548 (2015).
22. Nauck, M. A. et al. Glucagon-like peptide 1 inhibition of gastric emptying outweighs its insulinotropic effects in healthy humans. *Am. J. Physiol.* **273**, E981–E988 (1997).
23. Richards, P. et al. Identification and characterization of GLP-1 receptor-expressing cells using a new transgenic mouse model. *Diabetes* **63**, 1224–1233 (2014).
24. Hausch, F. Cryo-EM structures of class B GPCR reveal the activation mechanism. *Angew. Chem. Int. Ed. Engl.* **56**, 12412–12414 (2017).
25. Muller, T. D. et al. Glucagon-like peptide 1 (GLP-1). *Mol. Metab.* **30**, 72–130 (2019).
26. Cherney, D. Z. I. et al. Hemoglobin A1c reduction with the GLP-1 receptor agonist semaglutide is independent of baseline eGFR: post hoc analysis of the SUSTAIN and PIONEER programs. *Kidney Int. Rep.* **7**, 2345–2355 (2022).
27. Rodriguez, P. J. et al. Semaglutide vs tirzepatide for weight loss in adults with overweight or obesity. *JAMA Intern. Med.* **184**, 1056–1064 (2024).
28. Norgaard, C. H. et al. Treatment with glucagon-like peptide-1 receptor agonists and incidence of dementia: data from pooled double-blind randomized controlled trials and nationwide disease and prescription registers. *Alzheimers Dement. (N Y)* **8**, e12268 (2022).
29. Femminella, G. D. et al. Correction to: Evaluating the effects of the novel GLP-1 analogue liraglutide in Alzheimer's disease: study protocol for a randomised controlled trial (ELAD study). *Trials* **21**, 660 (2020).
30. Cai, H. Y. et al. Lixisenatide reduces amyloid plaques, neurofibrillary tangles and neuroinflammation in an APP/PS1/tau mouse model of Alzheimer's disease. *Biochem. Biophys. Res. Commun.* **495**, 1034–1040 (2018).
31. Duarte, A. I. et al. Liraglutide protects against brain amyloid-β_{1-42} accumulation in female mice with early Alzheimer's disease-like pathology by partially rescuing oxidative/nitrosative stress and inflammation. *Int. J. Mol. Sci.* **21**, 1746 (2020).
32. McClean, P. L. & Holscher, C. Lixisenatide, a drug developed to treat type 2 diabetes, shows neuroprotective effects in a mouse model of Alzheimer's disease. *Neuropharmacology* **86**, 241–258 (2014).
33. Kong, J., Wan, L., Wang, Y., Zhang, H. & Zhang, W. Liraglutide attenuates Aβ42 generation in APPswe/SH-SY5Y cells through the regulation of autophagy. *Neuropsychiatr. Dis. Treat.* **16**, 1817–1825 (2020).
34. Qing, H. et al. Valproic acid inhibits Aβ production, neuritic plaque formation, and behavioral deficits in Alzheimer's disease mouse models. *J. Exp. Med.* **205**, 2781–2789 (2008).
35. Ly, P. T. et al. Inhibition of GSK3β-mediated BACE1 expression reduces Alzheimer-associated phenotypes. *J. Clin. Invest.* **123**, 224–235 (2013).
36. He, M. et al. Identification and characterization of new long chain acyl-CoA dehydrogenases. *Mol. Genet. Metab.* **102**, 418–429 (2011).
37. Farzam, K. & Patel, P. Tirzepatide. *StatPearls* https://www.ncbi.nlm.nih.gov/books/NBK585056/ (2024).
38. Hawley, S. A. et al. Calmodulin-dependent protein kinase kinase-β is an alternative upstream kinase for AMP-activated protein kinase. *Cell Metab.* **2**, 9–19 (2005).
39. Shaw, R. J. et al. The tumor suppressor LKB1 kinase directly activates AMP-activated kinase and regulates apoptosis in response to energy stress. *Proc. Natl Acad. Sci. USA* **101**, 3329–3335 (2004).
40. King, M. R. et al. Insulin deficiency, but not resistance, exaggerates cognitive deficits in transgenic mice expressing human amyloid and tau proteins. Reversal by Exendin-4 treatment. *J. Neurosci. Res.* **98**, 2357–2369 (2020).
41. Christensen, M. A. et al. Transcriptional regulation of BACE1, the β-amyloid precursor protein β-secretase, by Sp1. *Mol. Cell. Biol.* **24**, 865–874 (2004).
42. Chen, C. H. et al. Increased NF-κB signalling up-regulates BACE1 expression and its therapeutic potential in Alzheimer's disease. *Int. J. Neuropsychopharmacol.* **15**, 77–90 (2012).
43. Tanaka, Y., Chambers, J. K., Matsuwaki, T., Yamanouchi, K. & Nishihara, M. Possible involvement of lysosomal dysfunction in pathological changes of the brain in aged progranulin-deficient mice. *Acta Neuropathol. Commun.* **2**, 78 (2014).
44. Pang, J., Feng, J. N., Ling, W. & Jin, T. The anti-inflammatory feature of glucagon-like peptide-1 and its based diabetes drugs—therapeutic potential exploration in lung injury. *Acta Pharm. Sin. B* **12**, 4040–4055 (2022).
45. Zhang, F. et al. Recombinant human GLP-1 beinaglutide regulates lipid metabolism of adipose tissues in diet-induced obese mice. *iScience* **24**, 103382 (2021).
46. Petrovic, A. et al. The role of GLP1-RAs in direct modulation of lipid metabolism in hepatic tissue as determined using in vitro models of NAFLD. *Curr. Issues Mol. Biol.* **45**, 4544–4556 (2023).
47. Panagaki, T., Randi, E. B., Szabo, C. & Holscher, C. Incretin mimetics restore the ER-mitochondrial axis and switch cell fate towards survival in LUHMES dopaminergic-like neurons: implications for novel therapeutic strategies in Parkinson's disease. *J. Parkinsons Dis.* **13**, 1149–1174 (2023).
48. Nachawi, N., Rao, P. P. & Makin, V. The role of GLP-1 receptor agonists in managing type 2 diabetes. *Cleve. Clin. J. Med.* **89**, 457–464 (2022).

49. Nauck, M. A. & Meier, J. J. The incretin effect in healthy individuals and those with type 2 diabetes: physiology, pathophysiology, and response to therapeutic interventions. *Lancet Diabetes Endocrinol.* **4**, 525–536 (2016).
50. Hui, H., Farilla, L., Merkel, P. & Perfetti, R. The short half-life of glucagon-like peptide-1 in plasma does not reflect its long-lasting beneficial effects. *Eur. J. Endocrinol.* **146**, 863–869 (2002).
51. Egan, J. M., Clocquet, A. R. & Elahi, D. The insulinotropic effect of acute exendin-4 administered to humans: comparison of nondiabetic state to type 2 diabetes. *J. Clin. Endocrinol. Metab.* **87**, 1282–1290 (2002).
52. Blevins, T. et al. DURATION-5: exenatide once weekly resulted in greater improvements in glycemic control compared with exenatide twice daily in patients with type 2 diabetes. *J. Clin. Endocrinol. Metab.* **96**, 1301–1310 (2011).
53. Lietzau, G. et al. Dipeptidyl peptidase-4 inhibitors and sulfonylureas prevent the progressive impairment of the nigrostriatal dopaminergic system induced by diabetes during aging. *Neurobiol. Aging* **89**, 12–23 (2020).
54. Eren-Yazicioglu, C. Y., Yigit, A., Dogruoz, R. E. & Yapici-Eser, H. Can GLP-1 be a target for reward system related disorders? A qualitative synthesis and systematic review analysis of studies on palatable food, drugs of abuse, and alcohol. *Front. Behav. Neurosci.* **14**, 614884 (2020).
55. Spoleti, E. et al. Dopamine neuron degeneration in the ventral tegmental area causes hippocampal hyperexcitability in experimental Alzheimer's disease. *Mol. Psychiatry* **29**, 1265–1280 (2024).
56. Murari, G. et al. Prefrontal GABA levels correlate with memory in older adults at high risk for Alzheimer's disease. *Cereb. Cortex Commun.* **1**, tgaa022 (2020).
57. Hansen, H. H. et al. The GLP-1 receptor agonist liraglutide improves memory function and increases hippocampal CA1 neuronal numbers in a senescence-accelerated mouse model of Alzheimer's disease. *J. Alzheimers Dis.* **46**, 877–888 (2015).
58. Hansen, H. H. et al. The GLP-1 receptor agonist liraglutide reduces pathology-specific tau phosphorylation and improves motor function in a transgenic hTauP301L mouse model of tauopathy. *Brain Res.* **1634**, 158–170 (2016).
59. Nauck, M. A., Quast, D. R., Wefers, J. & Meier, J. J. GLP-1 receptor agonists in the treatment of type 2 diabetes—state-of-the-art. *Mol. Metab.* **46**, 101102 (2021).
60. Shen, R. et al. GLP-1 receptor agonist attenuates tubular cell ferroptosis in diabetes via enhancing AMPK-fatty acid metabolism pathway through macropinocytosis. *Biochim. Biophys. Acta Mol. Basis Dis.* **1870**, 167060 (2024).
61. Herzig, S. & Shaw, R. J. AMPK: guardian of metabolism and mitochondrial homeostasis. *Nat. Rev. Mol. Cell Biol.* **19**, 121–135 (2018).
62. Garcia, D. & Shaw, R. J. AMPK: mechanisms of cellular energy sensing and restoration of metabolic balance. *Mol. Cell* **66**, 789–800 (2017).
63. Salminen, A., Kaarniranta, K., Haapasalo, A., Soininen, H. & Hiltunen, M. AMP-activated protein kinase: a potential player in Alzheimer's disease. *J. Neurochem.* **118**, 460–474 (2011).
64. Ou, Z. et al. Metformin treatment prevents amyloid plaque deposition and memory impairment in APP/PS1 mice. *Brain Behav. Immun.* **69**, 351–363 (2018).
65. Kuehn, B. M. In Alzheimer research, glucose metabolism moves to center stage. *JAMA* **323**, 297–299 (2020).
66. Willette, A. A. et al. Association of insulin resistance with cerebral glucose uptake in late middle-aged adults at risk for Alzheimer disease. *JAMA Neurol.* **72**, 1013–1020 (2015).
67. He, C. et al. Recurrent moderate hypoglycemia accelerates the progression of Alzheimer's disease through impairment of the TRPC6/GLUT3 pathway. *JCI Insight* **7**, e154595 (2022).
68. Fontanella, R. A. et al. Tirzepatide prevents neurodegeneration through multiple molecular pathways. *J. Transl. Med.* **22**, 114 (2024).
69. Yu, J. et al. IGF-1 induces hypoxia-inducible factor 1α-mediated GLUT3 expression through PI3K/Akt/mTOR dependent pathways in PC12 cells. *Brain Res.* **1430**, 18–24 (2012).
70. Jin, N. et al. CREB regulates the expression of neuronal glucose transporter 3: a possible mechanism related to impaired brain glucose uptake in Alzheimer's disease. *Nucleic Acids Res.* **41**, 3240–3256 (2013).
71. Halling, J. F. & Pilegaard, H. PGC-1α-mediated regulation of mitochondrial function and physiological implications. *Appl. Physiol. Nutr. Metab.* **45**, 927–936 (2020).
72. Ashleigh, T., Swerdlow, R. H. & Beal, M. F. The role of mitochondrial dysfunction in Alzheimer's disease pathogenesis. *Alzheimers Dement.* **19**, 333–342 (2023).
73. Blazquez, C., Woods, A., de Ceballos, M. L., Carling, D. & Guzman, M. The AMP-activated protein kinase is involved in the regulation of ketone body production by astrocytes. *J. Neurochem.* **73**, 1674–1682 (1999).
74. Thevenet, J. et al. Medium-chain fatty acids inhibit mitochondrial metabolism in astrocytes promoting astrocyte-neuron lactate and ketone body shuttle systems. *FASEB J.* **30**, 1913–1926 (2016).
75. Rojas-Morales, P., Pedraza-Chaverri, J. & Tapia, E. Ketone bodies, stress response, and redox homeostasis. *Redox Biol.* **29**, 101395 (2020).
76. Zhao, Z., Yan, J., Huang, L. & Yang, X. Phytochemicals targeting Alzheimer's disease via the AMP-activated protein kinase pathway, effects, and mechanisms of action. *Biomed. Pharmacother.* **173**, 116373 (2024).
77. Caberlotto, L., Lauria, M., Nguyen, T. P. & Scotti, M. The central role of AMP-kinase and energy homeostasis impairment in Alzheimer's disease: a multifactor network analysis. *PLoS ONE* **8**, e78919 (2013).
78. Fewlass, D. C. et al. Obesity-related leptin regulates Alzheimer's Aβ. *FASEB J.* **18**, 1870–1878 (2004).
79. Jantrapirom, S. et al. Liraglutide suppresses tau hyperphosphorylation, amyloid beta accumulation through regulating neuronal insulin signaling and BACE-1 activity. *Int. J. Mol. Sci.* **21**, 1725 (2020).
80. Yu, C. J. et al. The role of GLP-1/GIP receptor agonists in Alzheimer's disease. *Adv. Clin. Exp. Med.* **29**, 661–668 (2020).
81. Cao, B. et al. Neuroprotective effects of liraglutide against inflammation through the AMPK/NF-κB pathway in a mouse model of Parkinson's disease. *Metab. Brain Dis.* **37**, 451–462 (2022).
82. Zheng, Z. et al. Glucagon-like peptide-1 receptor: mechanisms and advances in therapy. *Signal Transduct. Target. Ther.* **9**, 234 (2024).
83. Lu, G. et al. AMPK activation attenuates central sensitization in a recurrent nitroglycerin-induced chronic migraine mouse model by promoting microglial M2-type polarization. *J. Headache Pain* **25**, 29 (2024).
84. Bard, F. et al. Peripherally administered antibodies against amyloid β-peptide enter the central nervous system and reduce pathology in a mouse model of Alzheimer disease. *Nat. Med.* **6**, 916–919 (2000).
85. Wang, W. et al. Associations of semaglutide with first-time diagnosis of Alzheimer's disease in patients with type 2 diabetes: target trial emulation using nationwide real-world data in the US. *Alzheimers Dement.* **20**, 8661–8672 (2024).
86. Zhang, Q. et al. *Contactin-associated protein-like 2* (*CNTNAP2*) mutations impair the essential α-secretase cleavages, leading to autism-like phenotypes. *Signal Transduct. Target. Ther.* **9**, 51 (2024).

87. Sun, X. et al. Hypoxia facilitates Alzheimer's disease pathogenesis by up-regulating *BACE1* gene expression. *Proc. Natl Acad. Sci. USA* **103**, 18727–18732 (2006).
88. Feng, Y. et al. Inhibition of IFITM3 in cerebrovascular endothelium alleviates Alzheimer's-related phenotypes. *Alzheimers Dement.* **21**, e14543 (2025).
89. Ly, P. T., Cai, F. & Song, W. Detection of neuritic plaques in Alzheimer's disease mouse model. *J. Vis. Exp.* **26**, 2831 (2011).

Acknowledgements

This work was supported by grants from the National Natural Science Foundation of China (numbers 82293642 and 82230043 to W.S. and 82201576 to Yun Z.), the Key Laboratory of Alzheimer's Disease of Zhejiang Province (ZJAD-2021004 to Yun Z.) and STI2030-Major Projects (2022ZD0211800 to Yun Z.). The funders had no role in study design, data collection and analysis, preparation of the manuscript or decision to publish.

Author contributions

Yun Z. and W.S. conceived and designed the experiments. Yun Z., H.C. and Y.F. performed most of the experiments. Yun Z., H.C. and Yang Z. did data analysis and figure editing. B.H., L.C., J.L., F.C., W.P., X.L. and I.B.-L. assisted with performing western blot experiments, plasmid construction, transfections and luciferase assay. Z.L. collected the blood samples from patients with AD and did the ^{18}F-AV45 PET/MD scans. M.L., B.H., Yifan Z. and Y.W. performed the genotyping and behavioral tests. Yun Z. and W.S. supervised the project, analyzed all the data and wrote the paper. Yun Z., H.C. and Y.F. are designated as co-first authors due to their substantial contributions to conducting experiments and analyzing data. Yun Z. is listed first for her input to the conception of the study and her contributions to writing the paper. All authors reviewed the paper.

Competing interests

The authors declare no competing interests.

Additional information

Extended data is available for this paper at https://doi.org/10.1038/s43587-025-00869-3.

Supplementary information The online version contains supplementary material available at https://doi.org/10.1038/s43587-025-00869-3.

Correspondence and requests for materials should be addressed to Yun Zhang or Weihong Song.

Peer review information *Nature Aging* thanks Christian Hölscher, Tami Rubinek and Marc Schneeberger for their contribution to the peer review of this work.

Reprints and permissions information is available at www.nature.com/reprints.

Publisher's note Springer Nature remains neutral with regard to jurisdictional claims in published maps and institutional affiliations.

[1]Department of Neurology, Nanjing Drum Tower Hospital, Affiliated Hospital of Medical School, Nanjing University, Nanjing, China. [2]National Clinical Research Center for Geriatric Disease, Xuanwu Hospital, Capital Medical University, Beijing, China. [3]The Second Affiliated Hospital and Yuying Children's Hospital, Zhejiang Key Laboratory of Alzheimer's Disease, Zhejiang Provincial Clinical Research Center for Mental Disorders, Wenzhou Medical University, Wenzhou, China. [4]Oujiang Laboratory (Zhejiang Lab for Regenerative Medicine, Vision and Brain Health), Center for Geriatric Medicine and Institute of Aging, The First Affiliated Hospital, Wenzhou Medical University, Wenzhou, China. [5]Chongqing Key Laboratory of Translational Medical Research in Cognitive Development and Learning and Memory Disorders, Ministry of Education Key Laboratory of Child Development and Disorders, Children's Hospital of Chongqing Medical University, Chongqing, China. [6]Department of Nuclear Medicine, The First Affiliated Hospital, Dalian Medical University, Dalian, China. [7]National Center for Neurological Disorders, Xuanwu Hospital, Capital Medical University, Beijing, China. [8]Department of Geriatric Neurology, Xiangya Hospital, Central South University, Changsha, China. [9]Townsend Family Laboratories, Department of Psychiatry, Brain Research Center, University of British Columbia, Vancouver, British Columbia, Canada. [10]These authors contributed equally: Yun Zhang, Huaqiu Chen, Yijia Feng. ✉e-mail: zhangyun_202104@163.com; weihong@wmu.edu.cn

nature portfolio

Corresponding author(s): Weihong Song, Yun Zhang

Last updated by author(s): Feb 26, 2025

Reporting Summary

Nature Portfolio wishes to improve the reproducibility of the work that we publish. This form provides structure for consistency and transparency in reporting. For further information on Nature Portfolio policies, see our Editorial Policies and the Editorial Policy Checklist.

Statistics

For all statistical analyses, confirm that the following items are present in the figure legend, table legend, main text, or Methods section.

n/a	Confirmed
☐	☒ The exact sample size (*n*) for each experimental group/condition, given as a discrete number and unit of measurement
☐	☒ A statement on whether measurements were taken from distinct samples or whether the same sample was measured repeatedly
☐	☒ The statistical test(s) used AND whether they are one- or two-sided *Only common tests should be described solely by name; describe more complex techniques in the Methods section.*
☐	☒ A description of all covariates tested
☐	☒ A description of any assumptions or corrections, such as tests of normality and adjustment for multiple comparisons
☐	☒ A full description of the statistical parameters including central tendency (e.g. means) or other basic estimates (e.g. regression coefficient) AND variation (e.g. standard deviation) or associated estimates of uncertainty (e.g. confidence intervals)
☐	☒ For null hypothesis testing, the test statistic (e.g. *F*, *t*, *r*) with confidence intervals, effect sizes, degrees of freedom and *P* value noted *Give P values as exact values whenever suitable.*
☒	☐ For Bayesian analysis, information on the choice of priors and Markov chain Monte Carlo settings
☐	☒ For hierarchical and complex designs, identification of the appropriate level for tests and full reporting of outcomes
☐	☒ Estimates of effect sizes (e.g. Cohen's *d*, Pearson's *r*), indicating how they were calculated

Our web collection on statistics for biologists contains articles on many of the points above.

Software and code

Policy information about availability of computer code

Data collection	*Provide a description of all commercial, open source and custom code used to collect the data in this study, specifying the version used OR state that no software was used.*
Data analysis	We used the NeuroQ software version 3.7

For manuscripts utilizing custom algorithms or software that are central to the research but not yet described in published literature, software must be made available to editors and reviewers. We strongly encourage code deposition in a community repository (e.g. GitHub). See the Nature Portfolio guidelines for submitting code & software for further information.

Data

Policy information about availability of data

All manuscripts must include a data availability statement. This statement should provide the following information, where applicable:

- Accession codes, unique identifiers, or web links for publicly available datasets
- A description of any restrictions on data availability
- For clinical datasets or third party data, please ensure that the statement adheres to our policy

The RNA-seq raw data are deposited in the the Sequence Read Archive (https://www.ncbi.nlm.nih.gov/sra) with BioProjectID (PRJNA1227686); SRA (SRR32510895, SRR32510896, SRR32510897, SRR32510898, SRR32510899 and SRR32510900). All other data are available from the corresponding author upon reasonable request.

Research involving human participants, their data, or biological material

Policy information about studies with human participants or human data. See also policy information about sex, gender (identity/presentation), and sexual orientation and race, ethnicity and racism.

Reporting on sex and gender	six male patients and six female patients. Similar findings are reported for both sex.
Reporting on race, ethnicity, or other socially relevant groupings	Chinese
Population characteristics	All individuals included in the study were over the age of 60 and diagnosed with Alzheimer's Disease.
Recruitment	Alzheimer's disease was diagnosed by at least two specialists, following the criteria of NINCDs-ADRDA. All participants underwent a comprehensive collection of medical history and clinical examination of the nervous system. Patients were excluded based on the following criteria: 1) Clinical conditions such as diabetes mellitus, epilepsy, stroke, or long-term use of medications known to cause progressive cognitive dysfunction; 2) Hachinski Ischemic Score (HIS) > 4 points, Hamilton Anxiety Rating Scale (HAMA) score ≥ 7 points, Hamilton Depression Rating Scale (HAMD) score ≥ 7 points; 3) Presence of severe heart, liver, lung, kidney or other organ diseases.
Ethics oversight	The study was approved by the Ethics Committee of the First Affiliated Hospital of Dalian Medical University (PJ-KS-KY-2023-149).

Note that full information on the approval of the study protocol must also be provided in the manuscript.

Field-specific reporting

Please select the one below that is the best fit for your research. If you are not sure, read the appropriate sections before making your selection.

☒ Life sciences ☐ Behavioural & social sciences ☐ Ecological, evolutionary & environmental sciences

For a reference copy of the document with all sections, see nature.com/documents/nr-reporting-summary-flat.pdf

Life sciences study design

All studies must disclose on these points even when the disclosure is negative.

Sample size	Human study: 12 patients; Animal study:52 transgenic mice. No statistical methods were used to pre-determine sample sizes but our sample sizes are similar to those reported in previous publication
Data exclusions	none
Replication	All experiments have been successfully replicated at least three times.
Randomization	Yes
Blinding	For our study, it was not required to perform data collection and analyses blind to the experimental conditions.

Reporting for specific materials, systems and methods

We require information from authors about some types of materials, experimental systems and methods used in many studies. Here, indicate whether each material, system or method listed is relevant to your study. If you are not sure if a list item applies to your research, read the appropriate section before selecting a response.

Materials & experimental systems

n/a	Involved in the study
☐	☒ Antibodies
☐	☒ Eukaryotic cell lines
☒	☐ Palaeontology and archaeology
☐	☒ Animals and other organisms
☒	☐ Clinical data
☒	☐ Dual use research of concern
☒	☐ Plants

Methods

n/a	Involved in the study
☒	☐ ChIP-seq
☒	☐ Flow cytometry
☒	☐ MRI-based neuroimaging

Antibodies

Antibodies used	Rabbit anti-APP C-terminal polyclonal antibody C20 was used to detect APP and its CTF products. BACE1 was detected with the anti-BACE1 antibody 208 recognizing the C-terminal end (Abcam, Cat#ab183612). Total AMPK was determined using a rabbit anti-AMPKα antibody (Cell Signaling Technology, Cat#2532S). Phosphorylated AMPK was determined using a rabbit anti-phospho-AMPKα (Thr172) antibody (Cell Signaling Technology, Cat#2535S). The NF-κB p65 subunit was determined using mouse anti-p65 (Sigma-Aldrich, Cat#8242S). GLP-1 receptors were determined using mouse monoclonal anti-GLP-1R antibody (Santa Cruz Biotechnology, Cat#sc-390774). CaMKK2 and LKB1 expressions were determined using rabbit anti-CaMKK2 antibody (Cell Signaling Technology, Cat#16810S) and rabbit anti-LKB1 antibody (Thermo Fisher Scientific, Cat#PA5-96062), respectively. CD68 was determined by rabbit anti-CD68 antibody (Proteintech, Cat#28058-1-AP). LAMP1 was determined by rabbit anti-LAMP1 antibody (Cell Signaling Technology, Cat#99437S). GLUT3 and PGC-1-α were determined by rabbit polyclonal anti-GLUT3 antibody (Proteintech, Cat#20403-1-AP) and mouse monoclonal anti-PGC-1-α antibody (Proteintech, Cat#66369-1-Ig). Internal control β-actin was analyzed using monoclonal antibody AC-15 (Sigma-Aldrich, Cat#A5441).
Validation	All antibodies used in the study have been validated, and the relevant validation information is available on the manufacturers' websites.

Eukaryotic cell lines

Policy information about cell lines and Sex and Gender in Research

Cell line source(s)	HEK293 (human embryonic kidney), N2a (mouse neuroblasts) and BV2 (mouse microglial) cells
Authentication	Short tandem repeat (STR) profiling was conducted for HEK and N2a cells to confirm their genetic identity. Immunocytochemistry or flow cytometry was also performed to check the cell-specific markers, BV2 cells (Iba1)
Mycoplasma contamination	The cells were tested and shown as negative for mycoplasma contamination
Commonly misidentified lines (See ICLAC register)	None

Animals and other research organisms

Policy information about studies involving animals; ARRIVE guidelines recommended for reporting animal research, and Sex and Gender in Research

Laboratory animals	APP23/PS45 mice were generated by crossing APP23 mice with mice overexpressing the human G384A-mutated PS1. The mice were used at 6 weeks of age. Mice were housed under controlled environmental conditions, including a 12-hour light/dark cycle (lights on at 7:00 AM and off at 7:00 PM), an ambient temperature of 22 ± 2°C, and a relative humidity of 50 ± 10%. These conditions were maintained to ensure the well-being and consistency of the experimental animals throughout the study.
Wild animals	none
Reporting on sex	26 male and 26 female
Field-collected samples	none
Ethics oversight	All animal experimental protocols were conducted in accordance with the regulations of the Institutional Animal Care and Use Committee of Wenzhou Medical University.

Note that full information on the approval of the study protocol must also be provided in the manuscript.

Plants

Seed stocks	*Report on the source of all seed stocks or other plant material used. If applicable, state the seed stock centre and catalogue number. If plant specimens were collected from the field, describe the collection location, date and sampling procedures.*
Novel plant genotypes	*Describe the methods by which all novel plant genotypes were produced. This includes those generated by transgenic approaches, gene editing, chemical/radiation-based mutagenesis and hybridization. For transgenic lines, describe the transformation method, the number of independent lines analyzed and the generation upon which experiments were performed. For gene-edited lines, describe the editor used, the endogenous sequence targeted for editing, the targeting guide RNA sequence (if applicable) and how the editor was applied.*
Authentication	*Describe any authentication procedures for each seed stock used or novel genotype generated. Describe any experiments used to assess the effect of a mutation and, where applicable, how potential secondary effects (e.g. second site T-DNA insertions, mosiacism, off-target gene editing) were examined.*